Contrib Mineral Petrol (2016) 171:60
DOI 10.1007/s00410-016-1265-5

ORIGINAL PAPER

Confort 15 model of conduit dynamics: applications to Pantelleria Green Tuff and Etna 122 BC eruptions

S. Campagnola[1] · C. Romano[1] · L. G. Mastin[2] · A. Vona[1]

Received: 20 August 2015 / Accepted: 10 May 2016 / Published online: 17 June 2016

Abstract Numerical simulations are useful tools to illustrate how flow parameters and physical processes may affect eruption dynamics of volcanoes. In this paper, we present an updated version of the *Conflow* model, an open-source numerical model for flow in eruptive conduits during steady-state pyroclastic eruptions (Mastin and Ghiorso in A numerical program for steady-state flow of magma-gas mixtures through vertical eruptive conduits. U.S. Geological Survey Open File Report 00-209, 2000). In the modified version, called *Confort 15*, the rheological constraints are improved, incorporating the most recent constitutive equations of both the liquid viscosity and crystal-bearing rheology. This allows all natural magma compositions, including the peralkaline melts excluded in the original version, to be investigated. The crystal-bearing rheology is improved by computing the effect of strain rate and crystal shape on the rheology of natural magmatic suspensions and expanding the crystal content range in which rheology can be modeled compared to the original version (*Conflow* is applicable to magmatic mixtures with up to 30 vol% crystal content). Moreover, volcanological studies of the juvenile products (crystal and vesicle size distribution) of the investigated eruption are directly incorporated into the modeling procedure. Vesicle number densities derived from textural analyses are used to calculate, through Toramaru equations, maximum decompression rates experienced during ascent. Finally, both degassing under equilibrium and disequilibrium conditions are considered. This allows considerations on the effect of different fragmentation criteria on the conduit flow analyses, the maximum volume fraction criterion ("porosity criterion"), the brittle fragmentation criterion and the overpressure fragmentation criterion. Simulations of the pantelleritic and trachytic phases of the Green Tuff (Pantelleria) and of the Plinian Etna 122 BC eruptions are performed to test the upgrades in the *Confort 15* modeling. *Conflow* and *Confort 15* numerical results are compared analyzing the effect of viscosity, decompression rate, temperature, fragmentation criteria (critical strain rate, porosity and overpressure criteria) and equilibrium versus disequilibrium degassing in the magma flow along volcanic conduits. The equilibrium simulation results indicate that an increase in viscosity, a faster decompression rate, a decrease in temperature or the application of the porosity criterion in place of the strain rate one produces a deepening in fragmentation depth. Initial velocity and mass flux of the mixture are directly correlated with each other, inversely proportional to an increase in viscosity, except for the case in which a faster decompression rate is assumed. Taking into account up-to-date viscosity parameterization or input faster decompression rate, a much larger decrease in the average pressure along the conduit compared to previous studies is recorded, enhancing water exsolution and degassing. Disequilibrium degassing initiates only at very shallow conditions near the surface. Brittle fragmentation (i.e., depending on the strain rate criterion) in the pantelleritic Green Tuff eruption simulations is mainly a function

Communicated by Timothy L. Grove.

Electronic supplementary material The online version of this article (doi:10.1007/s00410-016-1265-5) contains supplementary material, which is available to authorized users.

✉ S. Campagnola
silvia.campagnola@hotmail.it

[1] Dipartimento di Scienze, Università degli Studi Roma Tre, Largo San Leonardo Murialdo 1, 00146 Rome, Italy

[2] U.S. Geological Survey, Cascades Volcano Observatory, 1300 SE Cardinal Court, Bldg. 10, Suite 100, Vancouver, Wash., USA

of the initial temperature. In the case of the Etna 122 BC Plinian eruption, the viscosity strongly affects the magma ascent dynamics along the conduit. Using *Confort 15*, and therefore incorporating the most recent constitutive rheological parameterizations, we could calculate the mixture viscosity increase due to the presence of microlites. Results show that these seemingly low-viscosity magmas can explosively fragment in a brittle manner. Mass fluxes resulting from simulations which better represent the natural case (i.e., microlite-bearing) are consistent with values found in the literature for Plinian eruptions (~10^6 kg/s). The disequilibrium simulations, both for Green Tuff and Etna 122 BC eruptions, indicate that overpressure sufficient for fragmentation (if present) occurs only at very shallow conditions near the surface.

Keywords Numerical models · Magma rheology · Explosive eruptions · Decompression rate

Introduction

The energy of the eruption and the eruptive style of a volcanic system depend on a complex interplay between several factors. Volatile composition and content, rheology, temperature, pressure and geometry of the volcanic system are among the most important parameters affecting magma ascent along volcanic conduits and eruptive processes. In general, as magma ascends toward Earth's surface, decompression reduces volatile solubility. If the concentration of dissolved volatiles exceeds the equilibrium solubility at a given pressure, the melt becomes supersaturated, a requirement for bubble nucleation and growth (Sparks and Wilson 1982). Exsolved volatiles allow for significant magma compressibility and buoyancy, ultimately making eruption possible in an interplay between processes of volatile exsolution, gas expansion and viscosity changes of the melt–crystal mixture (Pyle 1995; Gonnermann and Manga 2007). Exsolution affects rheological properties, increasing the viscosity of the liquid as it becomes progressively devoid of H_2O (Dingwell et al. 1996) and modifying the viscosity of the two-phase mixture in a complex way (Llewellin and Manga 2005). Volatile exsolution also promotes microlite crystallization, which in turn affects bubble growth and rheology, leading to a complex feedback between decompression, exsolution and crystallization (Gardner et al. 1996; Gonnermann and Manga 2012).

During the last 30 years, several physical models of magma ascent along volcanic conduits have been proposed. The first numerical model of volcanic conduit flow was presented by Wilson et al. (1980), who idealized the erupting mixture as a single homogeneous fluid whose properties were bulk averages of the individual phases. Wilson et al. (1980) neglected heat and mass transfer through the conduit walls, temperature changes within the conduit and variations in mixture viscosity associated with bubble growth or exsolution of gases. Since 1980, conduit flow models have been expanded to include separated flow between magma and gas, variations in viscosity, density and gas solubility with melt composition, gas loss to conduit walls or two-dimensional conduit flow (e.g., Valentine and Wohletz 1989; Dobran 1992; Mastin 1995; Papale et al. 1998; Melnik 2000; Mastin and Ghiorso 2000; Massol et al. 2001; Polacci et al. 2004; Costa et al. 2007; Gonnermann and Manga 2007; de' Michieli Vitturi et al. 2010; Dellino et al. 2010; Lev et al. 2012; Dioguardi et al. 2013; Kawaguchi et al. 2013).

All conduit dynamics simulations reveal that magma density and volatile content exert first-order controls on magma behavior; however, the addition of multiphase rheology to models also plays a significant role on magma ascent dynamics. Naturally occurring magmas are commonly composed of a mixture of a liquid phase and suspended crystals and bubbles, where the compositions and relative proportions of each are in continuous evolution during ascent and degassing. The rheological properties of this mixture can differ by several orders of magnitude compared to the behavior of a liquid of the same chemical composition. The past few decades have seen extensive research on the rheology of multiphase suspensions, providing important constraints on the highly nonlinear dynamics of conduit flow processes that control eruptions (e.g., Bagdassarov and Dingwell 1992, 1993; Llewellin and Manga 2005; Ishibashi and Sato 2007; Lavallée et al. 2007; Caricchi et al. 2008; Cordonnier et al. 2009; Costa et al. 2009; Ishibashi 2009; Vona et al. 2011, 2013; Picard et al. 2011, 2013; Mader et al. 2013). Many conduit flow models, however, do not incorporate these complex rheological behaviors. Further, the few advanced models that do provide a more accurate description of the physical processes occurring in the conduit lack the accessibility or user-friendly interfaces of more commonly used models.

In order to fill this gap, and to provide an easy to access operational tool, we have updated the *Conflow* model, an open-source numerical model for flow of magma and gas in eruptive conduits during steady-state pyroclastic eruptions (Mastin and Ghiorso 2000; Mastin 2002). The modified program, called *Confort 15*, is written in Fortran 90 and can be operated on any platform that has such a compiler.

In the *Confort 15* program, several updates were considered:

1. The rheological parameters of the model are improved, by inserting the most recent equations describing both the liquid viscosity and crystal-bearing rheology. The earliest models for predicting the viscosity of geologi-

cally relevant silicate melts, including the one applied in the original *Conflow* model, adopted a strictly Arrhenian temperature dependence and were based on a relatively small number of high-T experiments (for melts containing less than 70 wt% SiO_2). Here, we insert the most recent generation of multicomponent chemical models for predicting the viscosity of naturally occurring silicate melts, which adopt a non-Arrhenian T-dependence. With this improvement, *Confort 15* can be applied to all natural magma compositions, including the peralkaline melts excluded in the original version.

2. The evaluation of crystal-bearing rheology is improved by computing the effect of crystal shape on the rheology of natural magmatic suspensions and expanding the crystal content range in which it could originally be modeled (the original *Conflow* model is applicable to magmatic mixtures with up to 30 vol% crystal content). This improvement allows investigation of the effect of suspended crystals on magma viscosity, which can increase the viscosity through both hydrodynamic and mechanical interaction among solid particles.
3. Volcanological studies of the juvenile products (crystal and vesicle size distribution) of the investigated eruption are directly incorporated into the modeling procedure. Textural-derived vesicle number densities are used to estimate, through Toramaru (1995, 2006) equations, maximum decompression rates experienced during ascent.
4. Both degassing under equilibrium and disequilibrium conditions are considered. The effect of different fragmentation criteria on the conduit flow analyses is evaluated, in terms of maximum volume fraction criterion ("porosity criterion," e.g., Sparks 1978; Wilson et al. 1978; Houghton and Wilson 1989), brittle fragmentation criterion (Dingwell and Webb 1989; Papale 1999) and, wherever degassing under disequilibrium conditions is considered, overpressure fragmentation criterion (Alidibirov 1994; Spieler et al. 2004).

In order to quantify how much these upgrades affect the modeling of the conduit dynamics during magma ascent and to look at subtle effects of viscosity, perhaps overlooked in previous studies, both *Conflow* and *Confort 15* were applied to two natural cases, the Pantelleria Green Tuff eruption (the peralkaline rhyolitic ignimbrite opening and the trachytic ending phases; Orsi and Sheridan 1984) and the Etna 122 BC eruption (the Plinian C phase; Coltelli et al. 1998).

Background model (*Conflow*)

Conflow is described in detail by Mastin and Ghiorso (2000) and Mastin (2002). In here, main advantages of the modeling procedure together with its limitations are summarized. *Conflow* models flow in eruptive conduits by assuming that (1) the flow is steady, (2) the conduit is vertical and circular in cross section, (3) temperature, pressure and velocity are the same for all phases at a given depth, (4) fluxes of heat and gas through the conduit wall are negligible relative to their flux up the conduit, (5) syn-eruptive crystallization is not taken into account, (6) the flow is one-dimensional (i.e., flow properties at any depth can be averaged across the conduit's cross section), (7) no work is done between the flowing magma and the surroundings, (8) the gas consists only of H_2O, (9) gas exsolution maintains equilibrium with pressure in the conduit. A more detailed description of the assumption and limitation of the modeling procedure is reported in Supplementary material section.

Conflow takes into account computations based on governing equations for conservation of mass, momentum and energy combined to give the pressure gradient at each depth (for details Mastin and Ghiorso 2000). Magma is assumed to exit the vent at $M = 1$ (i.e., Mach number, choked flow conditions), and the program iteratively adjusts the initial velocity to meet this boundary condition. The mass flux is held constant at all points in the conduit, and gas and melt are assumed to move together with no heat or gas loss to the surrounding wall rock. Changes in temperature of the mixture are calculated from the energy equation (Eq. 4 of Mastin and Ghiorso 2000), in which changes in mixture enthalpy are balanced by changes in kinetic and elevation potential energy. The densities of the melt and gas are calculated using methods of Ghiorso and Sack (1995) and Haar et al. (1984), whereas the density of crystals is assumed constant (as input). *Conflow* calculates the viscosity for melts containing less than 70 wt% SiO_2 among the anhydrous components using the parameterization of Shaw (1972), which applies a relatively simple Arrhenian relationship with viscosity inversely proportional to absolute temperature. For more siliceous melts, *Conflow* uses the relation of Hess and Dingwell (1996), which considers more realistic, non-Arrhenian temperature dependence parameterization of viscosity and more accurately incorporates the effect of dissolved water. To account for the effects of crystallinity, *Conflow* uses the Marsh (1981) calibration of the Einstein–Roscoe equation, in which viscosity increases exponentially toward infinity as the crystal fraction in the melt approaches 60 vol%. Above the point at which the fragmentation occurs, *Conflow* uses the Dobran (1992) equation to calculate the viscosity. *Conflow* adopts the maximum volume fraction criterion of fragmentation ("porosity criterion," Sparks 1978), acknowledging that this is an oversimplification. According to this criterion, the fragmentation of the magmatic mixture occurs when the $v_g = 0.75$, because of melt film thinning.

With some modification to the Fortran routine, *Conflow* may also consider the brittle fragmentation criterion (Papale 1999), which provides the theoretical framework to determine the conditions for the magma fragmentation, based on the Maxwell relation (Maxwell 1866; Dingwell and Webb 1989; Papale 1999).

Model improvements (*Confort 15*)

In this study, we updated the original version of *Conflow* inserting more recent viscosity formulations and the decompression rates, using vesicle number density and Toramaru (1995, 2006) formulations, as inputs. Moreover, the possibility to apply a disequilibrium bubble growth mode and to use the overpressure fragmentation criterion was included. The vesicle number densities obtained from textural analyses are also used as input to calculate bubble radius, the capillary number and, at the disequilibrium, the exsolved gas volume fraction. In Supplementary material, we discuss several *Confort 15* assumptions, as, for example, the ability to input decompression rate in the appropriate position during the rise along the conduit. In spite of the limitations and approximations, we believe that the *Confort 15* program here presented is a useful tool to be used not only to predict eruption characteristics, but especially to illustrate how flow parameters and their variation may affect eruption dynamics.

The improvements operated in the programming will be separately discussed below.

Rheology

In *Confort 15,* the liquid viscosity of metaluminous, calc-alkaline magmas is calculated using the non-Arrhenian, temperature-dependent GRD model (Giordano et al. 2008; Eqs. S.1–S.3) for naturally occurring silicate melts at atmospheric pressure (10^5 Pa). For peralkaline compositions (SiO_2 > 59 % and ($Na_2O + K_2O$)/Al_2O_3 > 1), we adopt the Di Genova et al. (2013; Eq. S.4) parameterization for peralkaline melts, based on a modified Vogel–Fulcher–Tammann equation, accounting for the effect of water and composition.

In *Confort 15*, we are able to insert up to three different crystal phases with the relative crystal density (instead of one crystal phase in *Conflow* model) and the aspect ratio of each phase. We use the viscosity parameterization of Vona et al. (2011; Eqs. S.5–S.7), which takes into account not only the crystal content, but also the crystal shape and the average strain rate undergone by the suspension, as all are demonstrated to play primary roles in influencing the transport properties of magmas (see Mader et al. 2013 for a review). Due to its functional form, the Vona et al. (2011) viscosity equation can be used only for $\phi < \phi_m$ (i.e., maximum packing fraction), as viscosity increases exponentially toward infinity as the crystal volume fraction approaches ϕ_m. In the case where $\phi > \phi_m$, *Confort 15* considers Costa et al. (2009; Eq. S.8) model that takes into account the shear rate ($\dot{\gamma}$) dependence of the suspension rheology. With some minor modifications to the source code (see the program manual in HUB), *Confort 15* is capable of using Costa et al. 2009 equation even below the maximum packing fraction allowing for instance to perform simulations below and above the maximum packing fraction using the same parameterization (Vona et al. 2011, as close packing is approached, goes to infinity and cannot be utilized).

Decompression rates

In *Confort 15,* an input decompression rate calculated using vesicle number densities (VNDs, i.e., number of vesicles per unit volume of melt) of eruptive products (Toramaru 1995) is inserted. If magma properties are known, VNDs can be translated directly into decompression rates. As in Mourtada-Bonnefoi and Laporte (2004), Cluzel et al. (2008), Shea et al. (2011) and Pardo et al. (2014), this conversion is achieved using the equations presented in Toramaru (2006):

$$\mathrm{Nv_{calc}} = 34X_0\left(\frac{16\pi\sigma^3}{3kTP_0^2}\right)^{-2}\left(\frac{\Omega_M P_0}{kT}\right)^{-1/4}\left(\frac{kTX_0DP_0^2}{4\sigma^2\left|\frac{\mathrm{d}P}{\mathrm{d}t}\right|}\right)^{-3/2} \quad (1)$$

where X_0 is the initial water concentration at the saturation pressure, dP/dt is the decompression rate, k is the Boltzmann constant, Ω_M is the volume of water molecules in the melt taken as 2.6×10^{-29} m^3, P_0 is the initial pressure, T the temperature in Kelvin, σ the surface tension and D the water diffusivity dependent primarily on temperature and dissolved water content in melt (e.g., Zhang and Behrens 2000).

In order to capture the decompression rates corresponding to the final stages of rapid ascent prior to fragmentation (e.g., Toramaru 1995; Shea et al. 2011), we only used number densities calculated for the smallest size range (0.01–0.001 mm, chosen from the change in slope at the smallest size in the cumulative vesicle size distribution curve, see Supplementary material). Thus, in all equations for the calculation of the decompression rate, the initial pressure and water contents must be calculated according to Eq. S.10, and they are related to depth and P/T conditions at initiations of late-stage nucleation. In particular, we used the porosity value obtained by summing the contributions from all vesicles with sizes $L \geq 0.01$ mm to derive X_0 using FOAMS software (Shea et al. 2010a). All VNDs obtained from smallest vesicles were normalized to melt volume to account for gas expansion. The surface tension σ

depends on several factors such as chemical composition of the melt, water content and temperature. Surface tension is also different if homogeneous or heterogeneous nucleation is considered.

Various authors investigated the relationship between homogeneous and heterogeneous nucleation, and they found that in heterogeneous nucleation, the activation energy is reduced by a factor ϕ expressed as (Hurwitz and Navon 1994): $\phi = [(2 - \cos\theta)(1 + \cos\theta)^2]/4$, where θ is the wetting angle between bubble and crystal and they substituted the "homogeneous" surface tension with an "effective" surface tension σ_{EFF} that incorporates the activation energy reduction term expressed as $\sigma_{EFF} = \phi^{1/3}\,\sigma_{HOM}$. Different effective surface tension in different compositions, such as dacites, rhyolites and phonolites, spanning between 0.01 and 0.1 N/m, has been reported in the literature (Bagdassarov et al. 2000; Mangan and Sisson 2000; Mourtada-Bonnefoi and Laporte 2004; Massol and Koyaguchi 2005; Shea et al. 2011). Based on curves of number densities per unit volume as a function of ascent rate $\log(dP/dt)$ as predicted by the model of Toramaru (1995, 2006) for varying "effective" surface tensions (Fig. S1 of Supplementary material) and the literature data, different values of surface tension were utilized in our simulations as a function of anhydrous liquid composition and water content (see supplementary material for details).

Disequilibrium bubble growth

Confort 15 can simulate the magma ascent also assuming disequilibrium bubble growth conditions. As the viscous limit (i.e., Peclet number $Pe = \tau_{vis}/\tau_{dec} \gg 1$) is achieved during the magma rise, bubble growth ($\dot{R}$) follows a viscosity controlled law (Lensky et al. 2004):

$$\dot{R} = \exp\left(\frac{\hat{t}\tau_{dec}}{2\tau_{vis}}\right) \quad (2)$$

where $\hat{t} = t/\tau_{dec}$ is the nondimensional time, $\tau_{dec} = P/(dP/dt)$ is the decompression timescale and $\tau_{vis} = 4\eta/P$ is a measure of the viscous relaxation time. In the viscous limit, the gas pressure inside bubble P_{gas} can become significantly larger than the surrounding pressure, resulting in the build-up of overpressure (e.g., Lensky et al. 2004; Gonnermann and Manga 2007). If disequilibrium bubble growth conditions are reached, in *Confort 15*, P_{gas} is then derived as the sum of ambient pressure, surface tension σ and viscous stresses due to the deformation of the melt shell (Lensky et al. 2004):

$$P_{gas} = P + \frac{2\sigma}{R} + 4\frac{\dot{R}}{R}\eta \quad (3)$$

where R is the bubble radius.

In the disequilibrium mode, the overpressure fragmentation criterion is calculated based on Alidibirov (1994) and Spieler et al. (2004). According to these studies, fragmentation takes place when volatile overpressure exceeds the tensile strength of the melt σ_m and ruptures bubble walls ($\Delta P = \sigma_m/\phi$).

Application to natural systems

Two volcanic systems have been selected to illustrate the role of model updates in *Confort 15* on ascent dynamics. The steady-state approximation was applied for both systems, as both eruption durations were considered longer than magma ascent times from chamber to surface. We have chosen two different phases of the Green Tuff eruption of Pantelleria (the peralkaline *Member A* and the trachytic *Member H*) in order to evaluate how different liquid compositions and derived viscosity models (Eqs. S.1–S.4) affect the magma dynamics. Then, to ascertain the updated crystal-bearing rheology (Eqs S.5–S.8), the Plinian Etna 122 BC eruption has been selected, highlighting the role of the microlite crystallization. In both cases, the effect of using VND-derived decompression rate as input and the different fragmentation criteria have also been evaluated (Eq. 1). In all simulations, unless otherwise specified, the strain rate fragmentation (Papale 1999) and the equilibrium degassing mode are adopted.

Green tuff ignimbrite of Pantelleria

Understanding the mechanisms that cause the shift between large-scale explosive and mild effusive eruptions, as evidenced by the wide spectrum of eruptive styles and intensities, as well as the extended welding and large-scale rheomorphic structures commonly associated with silica-rich peralkaline magmas represents a fascinating and intriguing question in volcanology.

Pantelleria Island is the type locality of pantellerite an iron- and sodium-rich peralkaline rhyolite and represents an ideal location to investigate these processes. The 45 ka Green Tuff ignimbrite is the most representative and widely distributed ignimbrite unit exposed on the island of Pantelleria (Orsi and Sheridan 1984). The Green Tuff formation is chemically zoned from pantellerite to trachyte (Mahood 1984). Orsi and Sheridan (1984) subdivide the Green Tuff unit into eight members. Since that pioneering work, several authors have reviewed the stratigraphy, taking into account differences in chemistry, emplacement models, lithostratigraphic details, structural features and paleomagnetic studies (Williams 2010; Speranza et al. 2011; Lanzo et al. 2013; Catalano et al. 2014). In this work, we

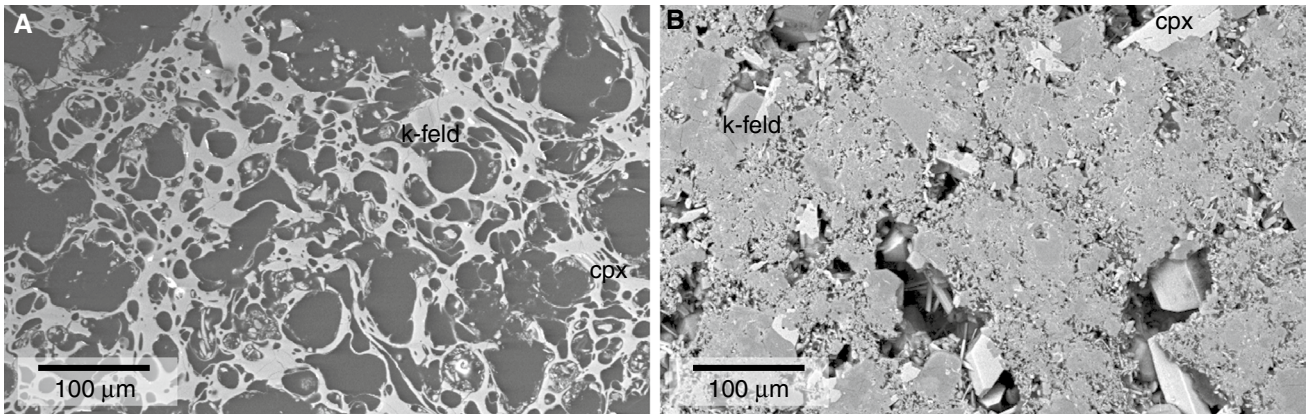

Fig. 1 Representative SEM BSE images for Green Tuff eruption **a** *Member A* and **b** *Member H*. k-feldspar (*dark gray*) and clinopyroxene (*light gray*) phases are indicated

considered the bottom and the top of the succession (hereafter *Member A* and *Member H* taking into account the Orsi and Sheridan (1984) stratigraphy, equivalent to Member A and Member E of Lanzo et al. (2013)), sampled in the proximity of the Lake Specchio di Venere (UTM 32 s, 766485 E, 4078986 N). *Member A* is a peralkaline Plinian-type pumice fall deposit at the base of the unit, restricted to the northeastern side of the island possibly due to a westerly prevailing wind at the time of eruption. *Member H* is a trachyte pyroclastic flow deposit, variably welded, with the highest quantity of free crystals and was inferred to cover the northwestern part of the island.

Textural characterization and decompression rates

The literature data on textural analysis of the Green Tuff eruption (Wolff and Wright 1981; Williams 2010; Neave et al. 2012; Lanzo et al. 2013) are sparse and do not allow us to derive maximum decompression rates experienced during ascent. Therefore, we performed textural analyses on samples taken from *Member A* and *H* of the succession. A description of the procedure used for density determination and sample imaging is summarized in Supplementary material. Microphotographs of representative samples are reported in Fig. 1. Crystal content varies significantly from early erupted (*Member A*) to late erupted (*Member H*), increasing from an average of $\phi = 0.08$ (phenocrysts) to $\phi = 0.33$ ($\phi = 0.23$ phenocrysts and $\phi = 0.10$ microlites), and the mineralogical assemblage is constituted by anorthoclase, clinopyroxene and rare magnetite and apatite. The calculated crystal aspect ratio (long axis/short axis) is about $R = 6$ for anorthoclase and $R = 3$ for clinopyroxene. Using Eq. (S.7), a mean weighted aspect ratio of $\bar{R} = 5$ can be estimated.

Quantification of the smallest vesicle size population (0.001–0.010 mm size range) reveals VNDs ranging between 2.3×10^8 cm^{-3} and 4.7×10^8 cm^{-3} for the *Member A* and between 1.6×10^7 cm^{-3} and 3.7×10^7 cm^{-3} for *Member H*. We calculated the decompression rates via the equations presented in Toramaru (1995, 2006, Eq. 1), using the obtained VNDs and considering appropriate values of diffusivity, density of the magma and surface tension. In particular, for *Member A* and *Member H,* respectively, we use water diffusivity of $D = 2 \times 10^{-12}$ m^2 s^{-1} and 4.3×10^{-11} m^2 s^{-1} calculated according to Zhang and Ni (2010), magma densities of 2680 and 2350 kg/m^3 from Bottinga and Weill (1970) and surface tension of 0.09 and 0.035 N/m (Cluzel et al. 2008; Gardner and Ketcham 2011). Inferred decompression rates are very fast at the beginning of the eruption (*Member A*), with an average value of 3.82 MPa/s (mirroring very high VNDs), and they decrease at the end of the eruption (*Member H*) with average of 1.82 MPa/s (lower VNDs).

Model input and output data analysis

Input parameters of both *A* and *H* Green Tuff members, derived from textural analysis and the literature data, are summarized in Table 1. For all simulations, we considered an initial $H_2O = 3$ wt% (Civetta et al. 1998; Lanzo et al. 2013), a cylindrical conduit 10 m in diameter and 4 km in depth (Civetta et al. 1998; Civile et al. 2008) and initial pressure as lithostatic at 100 MPa. Recent geochemical and petrological constraints indicate $T = 680$–800 °C as the more plausible eruptive temperature range for the pantelleritic *Member A* (White et al. 2009; Di Carlo et al. 2010; Lanzo et al. 2013) and $T = 950$ °C for the trachytic *Member H* (Wolff and Wright 1981; Lanzo et al. 2013). Therefore, unless otherwise specified, we assumed initial temperatures of $T = 750$ °C for the *Member A* and $T = 950$ °C for the *Member H* and we run simulations using the strain rate fragmentation criterion (Papale 1999). In Figs. 2 and

Table 1 Input data for the Green Tuff *Member A* and *Member H* performed simulations

Input Parameters	GT member A	GT member H
Chemical composition (wt%)[a]		
SiO_2	69.4	62.7
TiO_2	0.5	0.8
Al_2O_3	8.4	15.7
Fe_2O_3	8.6	6.3
MnO	0.3	0.2
MgO	0.1	0.2
CaO	0.4	1.1
Na_2O	6.3	7.1
K_2O	4.2	4.4
P_2O_5	–	0.2
Water content (wt%)[b]	3	3
Phenocrysts[c]		
Anorthoclase	0.05 (AR = 6)	0.18 (AR = 6)
Clinopyroxene	0.03 (AR = 3)	0.04 (AR = 3)
Microlites[c]		
Anorthoclase	–	0.05 (AR = 6)
Clinopyroxene	–	0.06 (AR = 3)
Temperature (°C)[d]	950/750	950
Initial pressure (MPa)[e]	100	100
Decompression rate (MPa/s)[f]	3.82	1.82
Conduit diameter (m)[g]	10	10
Conduit length (m)[g]	4000	4000

[a] Melt compositions from Williams (2010)

[b] Water content from Civetta et al. (1998) and Lanzo et al. (2013)

[c] Crystals (phenocrysts plus microlites) calculated in this study. In *Conflow*, phenocrysts and microlites are summed in a single phase and no aspect ratio (AR) is assigned

[d] Temperature from Wolff and Wright (1981), White et al. (2009), Di Carlo et al. (2010) and Lanzo et al. (2013)

[e] Initial pressure assumed as lithostatic (see text for details)

[f] Decompression rates calculated in this study, utilized only in *Confort 15*

[g] Conduit and length diameter from Civetta et al. (1998) and Civile et al. (2008)

3, different parameters are compared, such as gas volume fraction, viscosity, velocity and fragmentation depths. In order to highlight the effects of our software improvements (a–e in the list below), to evaluate the effect of the disequilibrium bubble growth (f), to estimate the effect of terminating exsolution at/after fragmentation (g) and to model the evolution of the Green Tuff eruption dynamics (h), several simulations were performed (Table 2) and the relative roles of variations in input parameters are discussed in subsections below. Each subsection presents a different comparison of model runs with a single change in input parameters.

Rheology

In order to estimate the role of different rheological parameterization, opening *Member A* and ending *Member H* of the Green Tuff eruption are simulated using both *Conflow* and *Confort 15* programs without explicit d*P*/d*t* input.

(a) Comparison of *Member A* GTA-C (*Conflow*) with GTA-1 (*Confort 15*) (Fig. 2, dashed and dotted green lines, respectively) shows several variations in flow properties during ascent. Differences in viscosity values are mostly related to the viscosities of the liquid phase. Shaw (1972) parameterization used in *Conflow* strongly overestimates viscosity for peralkaline liquids, as the strong influence of the alkali content on the overall viscosity of the peralkaline melt is not considered. In *Confort 15,* the Green Tuff *Member A* satisfies the agpaitic test described in Eq. (S.4), and thus, the model uses the Di Genova et al. (2013) equation. According to the authors' parameterization, silica-rich, peralkaline liquids such as the pantellerites have relatively high viscosities in the high-temperature range, in agreement with their low NBO/T, whereas in the low temperature range their viscosities decrease dramatically due to the excess of alkalis (AEX, Eq. S.4). In order to understand the differences in viscosity for different parameterizations, in Fig. 4a liquid viscosity values pertaining to the *Member A* at the eruptive temperature of 750 °C are reported as a function of the water content for different parameterizations (Shaw 1972; Di Genova et al. 2013). In this plot, crystal and vesicle effects on the rheology of the magma are not considered. At the initial water content of 3 wt% assumed in the simulations, the viscosity calculated by the Shaw (1972) parameterization (*Conflow*) is about half an order of magnitude higher (5.05 vs. 4.49 log units Pa s) than the viscosity computed by the Di Genova et al. (2013) equation (*Confort 15*). This discrepancy increases up to about 1 order of magnitude with decreasing water content (i.e., 1 wt%). The effect of crystals on the viscosity of the *Member A* is negligible because of the low average crystal content ($\phi = 0.08$). Both Einstein–Roscoe and Vona et al. (2011) equations, used in *Conflow* and *Confort 15,* respectively, yield a relative viscosity value of about 0.2 log units (Fig. 4c).

Differences in viscosities reflect variations in conduit dynamics (Fig. 2). In GTA-1 over GTA-C, lower viscosity at fragmentation ($10^{6.0}$ vs. $10^{6.7}$ Pa s) and consequent weaker frictional forces between the magma and the conduit walls yield an increase in the magma flow and mass flow rate (6.2×10^4 and 1.2×10^3 kg/s) and a

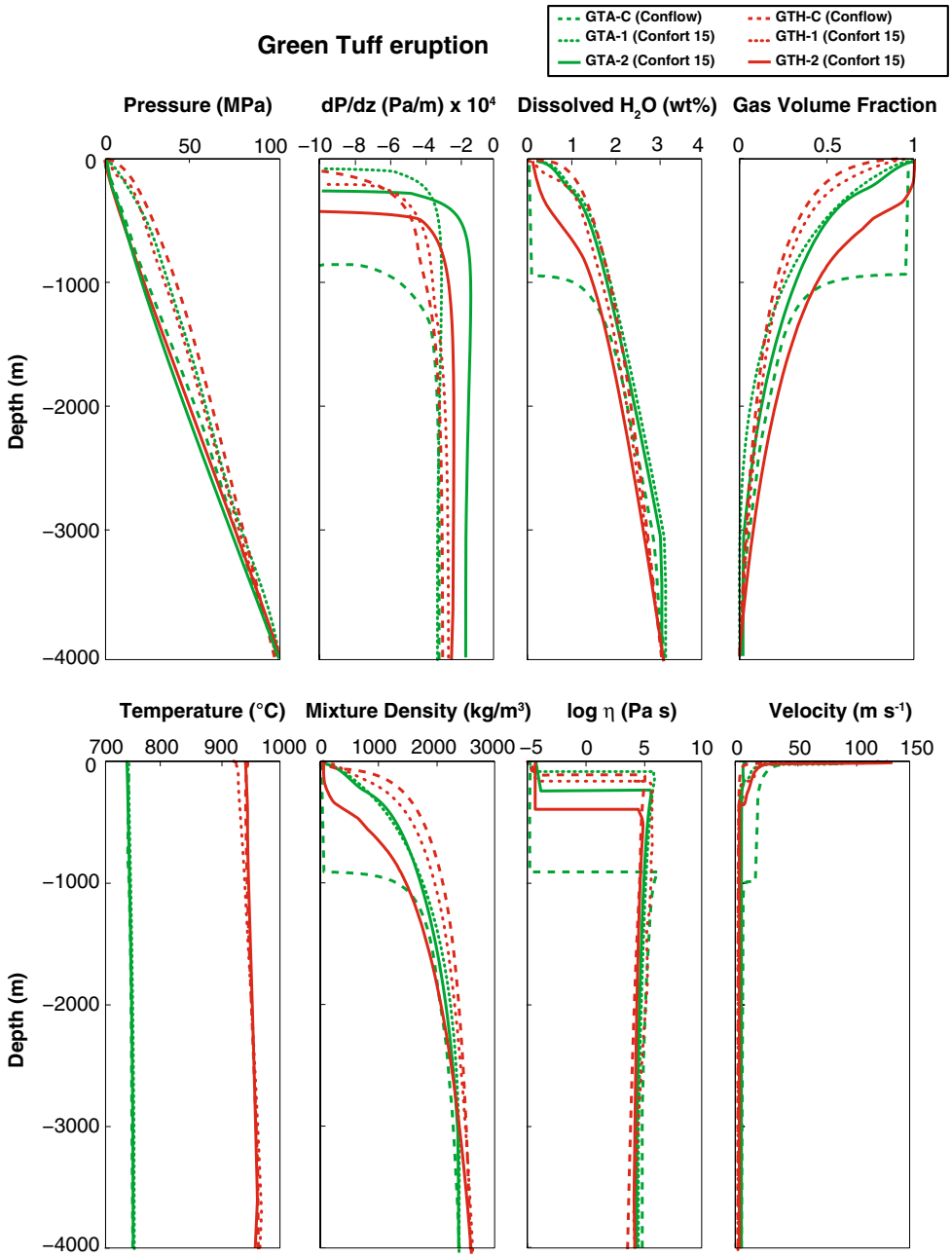

Fig. 2 Plot results for the simulations of Green Tuff *Member A* (*green lines*) and *Member H* (*red lines*): *Conflow* (*dashed lines*), *Confort 15* without input d*P*/d*t* (*dotted lines*) and *Confort 15* including d*P*/d*t* (*solid lines*) modeling results. Run conditions are: $H_2O_{init} = 3$ wt%, $T_{init} = 950$ °C, $P_{init} = 100$ MPa, conduit diameter = 10 m, conduit length = 4 km. Simulations are labeled according to Table 2

corresponding increase in the initial velocity as required to balance the distribution of forces acting on a batch of magma (momentum equation). The fragmentation depth also is inversely correlated with the viscosity, occurring shallower in the conduit in GTA-1 compared to GTA-C (120 vs. 900 m). Lower viscosities produce small heat loss and a higher average pressure within the conduit. High pressure values due to lower viscosity are maintained along the conduit before and after fragmentation and final higher pressure values are recorded (0.82 vs. 0.18 MPa) and they are clearly inversely correlated with the final residual water content (0.11 vs. 0.37 wt%). Furthermore, high pressure values decrease the rate of volatile exsolution and gas expansion, limiting the acceleration. As the original water content is identical in both cases, the balance of the final gas volume fraction and density (along with temperature) leads to identical choked flow velocity (91 m/s).

(b) Comparison of trachytic Green Tuff *Member H* GTH-C (*Conflow*) with GTH-1 (*Confort 15*) (Fig. 2, dashed and dotted red lines, respectively) is presented. In *Confort 15*, the Green Tuff *Member H* fails the agpaitic test described in Eq. (S.4), because it reaches

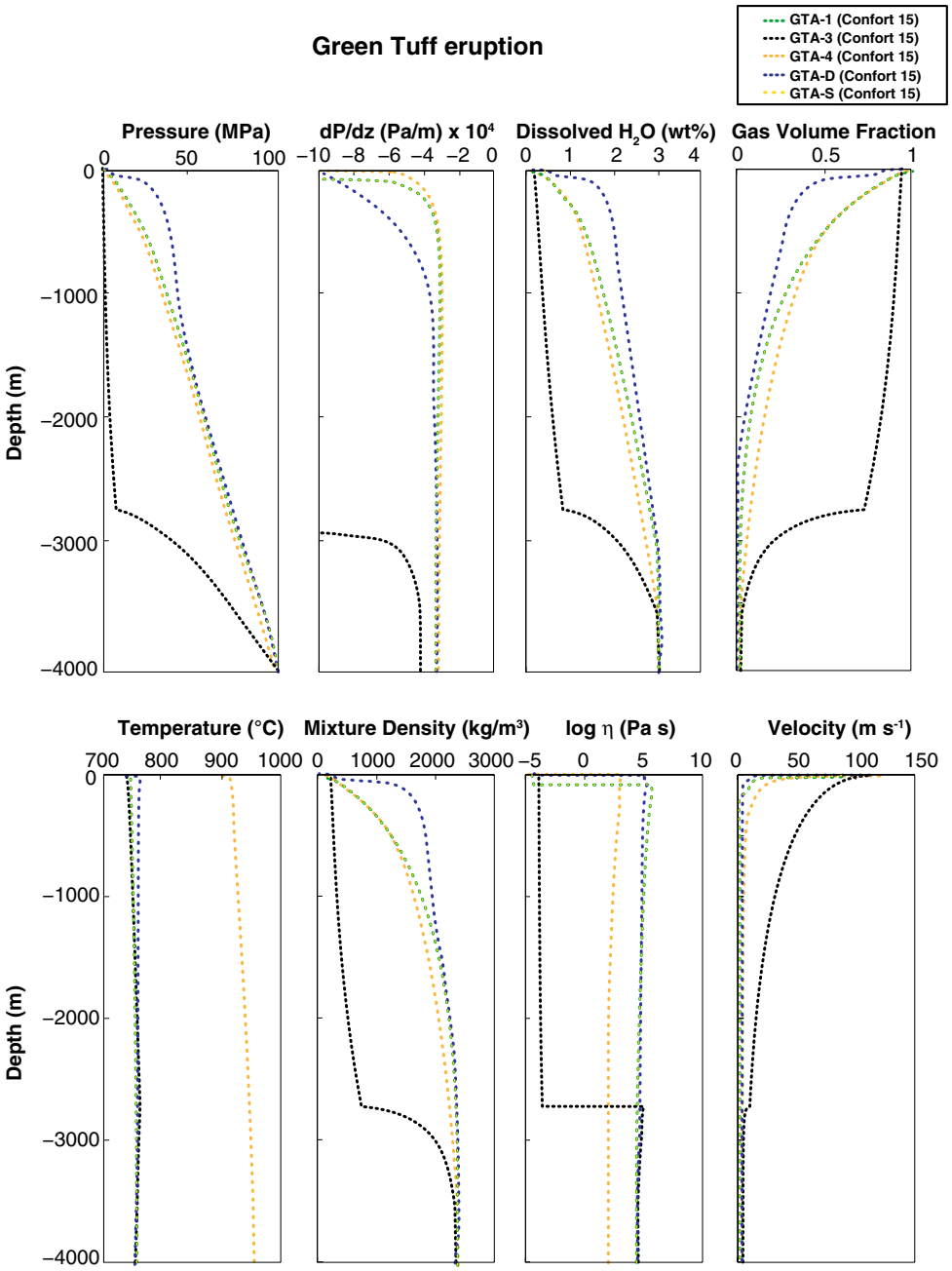

Fig. 3 Plot results for the simulations of Green Tuff *Member A* applying *Confort 15* program. Simulations are: $T = 750$ °C and strain rate criterion (*green*); $T = 750$ °C and porosity criterion (*black*); $T = 950$ °C and strain rate criterion (*orange*); $T = 750$ °C at the disequilibrium and overpressure criterion (*blue*); $T = 750$ °C and stop exsolution after fragmentation (*yellow*). Run conditions: $H_2O_{init} = 3$ wt%, $P_{init} = 100$ MPa, conduit diameter = 10 m, conduit length = 4 km. Simulations are labeled according to Table 2

agpaitic index of 0.68, far below the value of 1, which defines a peralkaline melt (*Member H* is trachytic in composition). Therefore, in this case, the program adopts the GRD equation (Giordano et al. 2008) to model the viscosity of the liquid. To help visualization, we plot liquid viscosity values pertaining to the *Member H* at the eruptive temperature of 950 °C as a function of the water content (Fig. 4B) applying Shaw (1972) and GRD (Giordano et al. 2008) parameterizations (*Conflow* vs. *Confort 15*). We can observe that at the initial water content of 3 wt% assumed in the simulations, the values of viscosity obtained using the two models are identical within error, with Shaw (1972) yielding slightly higher values compared to GRD. The curves show a small discrepancy (about 0.12 log units Pa s) for water contents down to 0.5 wt%. At even dryer conditions (<0.5 wt%), the GRD model strongly departs from Shaw (1972) with viscosity values up to about 6.3 log units Pa s (0.8 log units higher than values obtained using Shaw model). The crystal-bearing viscosity is noticeably different for the two parameterizations. The Vona et al. (2011) equation used in *Confort 15* (GTH-1) takes into account the

Table 2 Summary of main results for the Green Tuff eruption performed simulations (for details see text)

Simulation id	Sample	Program	Temperature (°C)	Fragmentation criterion	Decompression rate (MPa/s)	Mass flux (Kg/s)	Initial velocity (m/s)	Initial density (kg/m^3)	Fragmentation depth (m)	Maximum viscosity (log units Pa s)	Exit velocity (m/s)	Residual water (wt%)	Final pressure (MPa)	Final density (kg/m^3)	Exit gas volume fraction
GTA-C	Member A	Conflow	750	Strain rate	–	1.2×10^3	0.02	2400	900	6.7	91	0.11	0.18	13	0.99
GTA-1	Member A	Confort 15	750	Strain rate	–	6.2×10^4	0.03	2400	120	6.0	91	0.37	0.82	75	0.96
GTA-2	Member A	Confort 15	750	Strain rate	3.82	9.3×10^5	0.05	2400	240	5.9	93	0.27	0.69	52	0.98
GTA-3	Member A	Confort 15	750	0.75 porosity	–	4.0×10^5	2.17	2400	2700	5.9	116	0.58	0.98	172	0.94
GTA-4	Member A	Confort 15	950	Strain rate	–	4.9×10^7	2.74	2400	–	4.0	127	0.36	0.79	60	0.97
GTA-D	Member A	Confort 15	750	Overpressure	–	9.6×10^4	0.96	2400	10	5.4	114	0.56	0.99	89	0.94
GTA-S (se[a])	Member A	Confort 15	750	Strain rate	–	6.1×10^4	0.02	2400	110	6.0	88	0.41	0.82	73	0.97
GTH-C	Member H	Conflow	950	Strain rate	–	2.5×10^5	0.10	2600	115	5.0	128	0.32	0.14	42	0.95
GTH-1	Member H	Confort 15	950	Strain rate	–	1.1×10^4	0.06	2600	200	5.6	97	0.17	0.01	25	0.99
GTH-2	Member H	Confort 15	950	Strain rate	1.82	4.9×10^6	0.41	2600	490	5.4	135	0.15	0.00	16	0.99

[a] se = stop exsolution at/after fragmentation

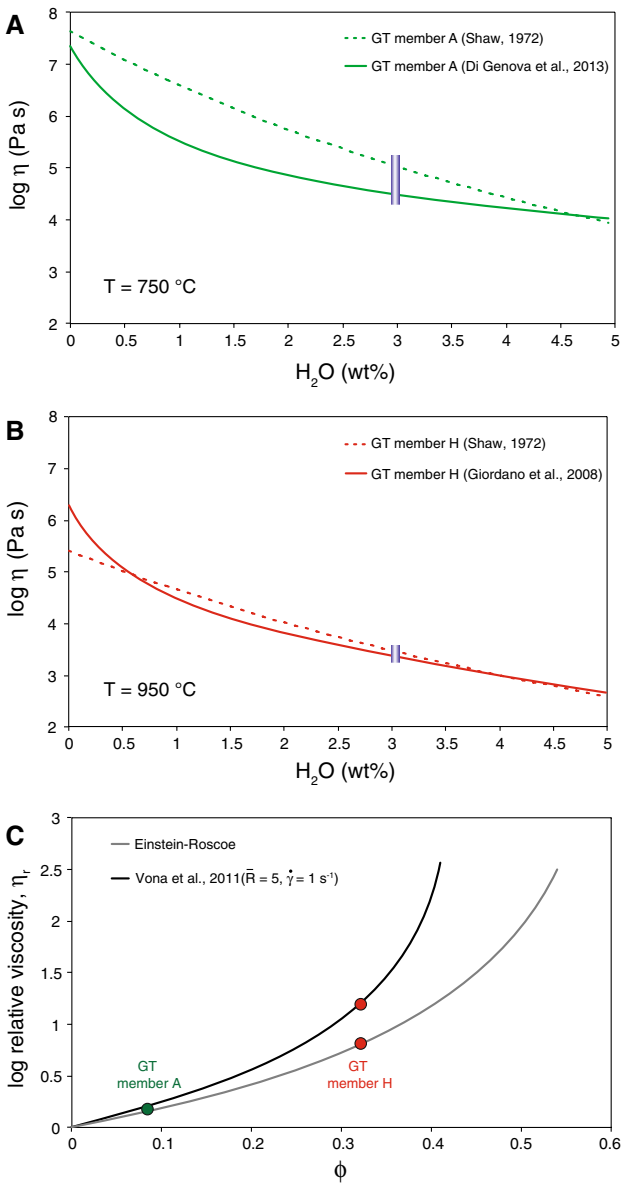

Fig. 4 Calculated liquid viscosity of the Pantellerite Green Tuff *Member A* (**a**) and *Member H* (**b**) as a function of the water content for all used viscosity parameterizations (Shaw 1972; Giordano et al. 2008; Di Genova et al. 2013). *Blue area* indicates initial H_2O content assumed in the simulations (3 wt%). **c** Relative viscosity of the multiphase magma as a function of crystal fraction (ϕ). *Gray line* describes the Einstein–Roscoe equation (ER), *black line* the model by Vona et al. (2011). *Circles* represent viscosity estimations based on measured crystallinity for the Green Tuff *Member A* (*green*) and *Member H* (*red*)

effect of crystal content, crystal shape and strain rate in the rheology of melt, and it gives more accurate results especially when elongated crystals are present. As can be seen from Fig. 4c, the elongated shape ($\bar{R} = 5$) of crystals produces a greater relative viscosity increase by about 0.4 log units.

This variation in viscosity affects the conduit dynamics (Fig. 2), leading to a twofold deepening in the fragmentation depth in GTH-1 over GTH-C (200 vs. 115 m). The maximum viscosity ($10^{5.6}$ vs. $10^{5.0}$ Pa s) is inversely correlated with the initial velocity, and the corresponding mass flux is about one order of magnitude lower (1.1×10^4 and 2.5×10^5 kg/s), as required to balance the mass and momentum equations. In GTH-1, higher viscosities calculated with the Vona et al. (2011) model are also correlated with lower average pressure along the conduit and at the vent, higher water exsolution and lower residual water content. Although the effect of viscosity on the physical parameters and their variation within the conduit is clear and consistent, exit velocities vary in less predictable pattern to match with viscosity variations, pressure distribution along the conduit and sonic conditions at the vent (choked flow). The latter depends on the density of the magmatic mixtures and on the bulk modulus and volume of gas, crystal and liquid phases. In this case, GTA-1 presents lower exit velocities (97 m/s) compared to the *Conflow* simulation, GTH-C (128 m/s), despite the lower density and the higher exit gas volume fraction of GTH-1 (99 vs. 95 %). It is interesting to note that fragmentation occurs for viscosities as low as 10^5 Pa s, which imply, for the brittle failure criterion, conditions of very rapid ascent along the conduit.

Decompression rate

(c) In order to estimate the role of explicit input of decompression rate on model runs of the Green Tuff *Member A*, a simulation using a d*P*/d*t* of 3.82 MPa/s (from Eq. (1); GTA-2, Fig. 2 solid green line) is compared to GTA-1 (*Confort 15* model, without input d*P*/d*t*, dotted green line). The faster input decompression rate of GTA-2 results in a slight deepening of the fragmentation depth as the brittle fragmentation criterion conditions are reached earlier during ascent (240 vs. 120 m). Initial velocities are linear with mass fluxes, greater by about one order of magnitude in GTA-2 than GTA-1 (9.3×10^5 vs. 6.2×10^4 kg/s), with important implications in terms of eruption dynamics and stability of the eruptive column. Higher decompression rates correspond to lower pressure distributions along the conduit and enhanced volatile exsolution, higher acceleration and higher initial velocities. Exit velocities are almost identical within error in the two simulations (93 vs. 91 m/s). For identical initial water contents, the final exit velocities depend on the temperature, the amount of exsolution and the gas fraction. The small differences in fragmentation depth, gas volume fraction, and density at the exit in the two simulations do not produce any remarkable difference in exit velocities, which remain almost identical for identical initial water content.

Fragmentation criteria

(d) To evaluate how much the different fragmentation criteria may affect the dynamics along the conduit, we run a simulation of the *Member A* in *Confort 15* using the alternative fragmentation criterion of 0.75 porosity threshold and we compare it to the equivalent simulation adopting strain rate criterion (GTA-3 vs. GTA-1 Fig. 3, dotted black and green lines, respectively). The input conditions are identical and simulations were run without imposing the decompression rate. Adopting the porosity criterion (GTA-3), fragmentation strongly deepens in the conduit (2700 vs.120 m) and initial velocity, mass flux (4×10^5 vs. 6.2×10^4 kg/s) and final pressure are all increased over the strain rate criterion, in agreement with previous simulations (e.g., Mastin 2002; Mangan et al. 2004). The different final pressures for GTA-3 over GTA-1 simulations are linear with the final densities (172 vs. 75 kg/m^3) and final residual water content (0.58 vs. 0.37 wt%). Exit velocities are higher in the GTA-3 case (116 vs. 91 m/s), due to a balance between densities and gas volume fraction (94 vs. 96 %) at the exit. The one-order higher mass flux in the porosity criterion case seems counterintuitive given its greater fragmentation depth. Because of the much higher fragmentation depth, for porosity criterion mixture (GTA-3) viscosity is much lower than for strain criterion (GTA-1) at porosities >0.75, and this leads to higher pressure at the exit, higher exit densities and hence higher mass eruption rate.

Temperature

(e) The effect of temperature in modifying flow properties along the conduit is evaluated by comparing *Confort 15* simulations at 950 and 750 °C (GTA-4 vs. GTA-1, Fig. 3, dotted orange and green line, respectively). It is important to note that temperature plays a key role in affecting magma properties and consequently conduit dynamics. GTA-4 simulation ($T = 950$ °C) yields lower maximum viscosities ($10^{4.0}$ vs. $10^{6.0}$ Pa s), and a corresponding variation of fragmentation conditions and eruptive style. In GTA-4, low viscosities prevent the achievement of fragmentation conditions, whereas in GTA-1 ($T = 750$ °C) brittle behavior occurs at 120 m. The decrease in viscosity and increase in T lead to a strong increase in initial velocity and three-times increase in mass flux (4.9×10^7 vs. 6.2×10^4 kg/s), to balance mass, energy and momentum equations. The effect of increasing temperature counteracts that of decreased viscosities in terms of gas exsolution, so that in the high-temperature simulations, a slightly higher decompression rate and lower pressure distribution along the conduit are encountered, correlated with higher exsolution and gas volume fraction both along the conduit and at the exit. Along the conduit, for the low T case (GTA-1) densities are always higher and gas volume fractions are always lower, so exsolution is retarded. Exit velocities are lower for the simulation at 750 °C (GTA-1) compared to the simulation run at 950 °C (GTA-4). Again, exit velocities are constrained by the Mach number and derive from a complex interplay among different parameters, which all act to modify the sound speed in the magmatic mixture. In this case, the higher temperature of GTA-4 yields higher acceleration along the conduit and lower densities, which could be responsible for the higher velocities at vent. Finally, it is very important to notice that a very important effect of high-temperature conditions (identical to those observed in the trachytic *Member H*) is to prevent fragmentation on the pantelleritic melt. We will comment later on this important issue.

Disequilibrium bubble growth

(f) In order to evaluate the bubble growth dynamics in magma during ascent, a set of simulations are performed using the disequilibrium mode (GTA-D Fig. 3, dotted blue line) and compared to the equivalent simulation at the equilibrium (GTA-1 Fig. 3, dotted green). In the disequilibrium mode, once the viscous limit is reached, testified by a very large Peclet number, *Confort 15* calculates the disequilibrium average bubble radius (Eqs. 2, 3). As the bubble growth is delayed, due to the viscous forces, overpressure in bubbles with respect to the surrounding liquid is developed.

To isolate the effect of disequilibrium degassing on flow properties, input decompression rate is not imposed. In GTA-D, the initial and final velocities are higher, conduit pressures are greater at comparable depths, and the mass flux is more than twice (9.6×10^4 vs. 6.2×10^4 kg/s). At the vent, the delayed bubble growth using disequilibrium equations (Eqs. 2, 3) leads to shallower fragmentation depth, and, in order to satisfy choked conditions at the vent, this results in higher initial and final velocities, higher pressure along the conduit, and a twofold increase in the residual water content (0.56 vs. 0.37 wt%), lower gas volume fraction (0.94 vs. 0.96 %) and higher density. As the viscous resistance retards bubble growth, the gas pressure inside the bubbles may exceed ambient pressure. In the disequilibrium simulation bubble overpressure meets the fragmentation threshold pressure at ~4 MPa and at shallower depth than the strain rate criterion for the equilibrium set (10 vs. 120 m). In general, however, according to Eqs. 2, 3, disequilibrium degassing initiates at very shallow conditions near the surface, at porosities on the order of 90 %. Fragmentation conditions are reached at even shallower depth in the conduit, at porosity of about 93 %. Fragmentation according to porosity and strain rate criteria both occurs before the onset of disequilibrium conditions, for porosities more comparable to values reported in textural studies. For

this reason, we suggest that the assumption of equilibrium degassing is reasonable and can be adopted for the modeling of the eruption dynamics discussed below.

Gas exsolution at/after fragmentation

(g) *Confort 15* allows the option of calculating continued exsolution above the fragmentation depth or terminating it at fragmentation level. In Fig. 3, a simulation of the Green Tuff *Member A* stopping exsolution after fragmentation (GTA-S, dotted yellow line) is compared to GTA-1 (dotted green line). The inhibition of exsolution after fragmentation of GTA-S results in a slight shallower fragmentation depth (110 vs. 120 m), almost identical initial velocities (0.02 v. 0.02 m/s) and mass fluxes (6.1×10^4 vs. 6.2×10^4 kg/s). The higher residual water content at the exit (0.41 vs. 0.37 wt%) and the inversely correlated exit gas volume fraction (0.97 vs. 0.96 %) lead to slightly lower exit velocities (88 vs. 91 m/s). In general, for the case of Green Tuff *Member A*, allowing exsolution to proceed after fragmentation or to terminate at fragmentation level does not produce any remarkable difference in eruptive dynamics.

Evolution of Green Tuff eruptive dynamics

(h) Using geologically constrained input parameters, we discuss differences in eruption with *Confort 15* updated model (GTA-2 vs. GTH-2, Fig. 2 green and red solid lines, respectively).

At the same temperature, despite its more evolved composition, the peralkaline signature of the *Member A* (pantellerite) yields lower liquid viscosities compared to that of *Member H* (trachyte). However, considering the distinctive temperature (T = 750 vs. 950 °C), decompression rate (dP/dt = 3.82 vs. 1.82 MPa/s) and crystal content (ϕ = 0.08 vs. 0.33), GTA-2 maximum viscosity is slightly higher than that of GTH-2 ($10^{5.9}$ vs. $10^{5.4}$ Pa s). Distinctive input conditions affect intrinsic parameters of the magma during ascent along the conduit, leading to differences in conduit dynamics and fragmentation depths. The higher viscosity of *Member A* is associated, as in the previous simulations, with slightly lower initial velocity and mass fluxes of about one order of magnitude lower (9.3×10^5 vs. 4.9×10^6 kg/s). The VND-based higher dP/dt of the *A* member of the eruption results in slightly lower average pressure for *Member A* along the conduit compared to *Member H*. The degree of exsolution and gas volume fraction is always lower along the conduit in *Member A* simulations, whereas the final pressure and residual water in the melt are higher than in *Member H* runs. Image-derived porosities compare well with porosities at fragmentation both for GTA-2 (78 vs. 82 %) and GTH-2 (81 vs. 88 %). Mixture density is also higher along the conduit and at the exit, at lower exsolution rate and lower temperature conditions in *Member A* over *Member H*. In this case, brittle failure is reached at twofold higher depth for the GTH-2 (higher velocities and higher strain rates) than GTA-2 (490 vs. 240 m). The GTA-2 is characterized by a mass flux of 9.3×10^5 kg/s, lower than the values reported in the literature from field and chemical studies (~2×10^8 kg/s Williams et al. 2013). It must be noted, however, that the values previously reported in the literature refer to the bulk of the eruptive sequence, considering therefore not only the localized pumice fallout (*Member A*) investigated here, but also the subsequent pyroclastic density current. It is known that generally the mass flux of highly explosive eruptions increases from the initial fallout phase to the initiation of pyroclastic fountaining and generation of pyroclastic density currents (e.g., Sparks 1978; Wilson et al. 1980; Bursik and Woods 1996). The increase in mass flux occurring toward the end of the eruption (*Member H*) is also correlated with the corresponding increase in temperature (White et al. 2009; Lanzo et al. 2013), and it is not easily reconciled with the expected waning of the eruption, under the assumption of a homogeneous pressurized finite volume source. Interpretation of the data in terms of eruptive sequence is hampered by the lack of data for the bulk of the eruption (only two phases of the eruptions are here considered), and therefore, further data are needed to completely assess the eruption dynamics. We want to stress that the exercise carried out in this study is focused on understanding how variations in updated input parameters may generally affect conduit dynamics and further study should be performed in order to attempt a complete characterization of the eruptive dynamics of this eruption.

Etna 122 BC

Unlike their silicic counterparts, basaltic volcanoes show a very wide spectrum of eruptive styles from common effusive to low-energy Strombolian and Hawaiian eruptions, to large-scale paroxysmal sub-Plinian and Plinian events. The most powerful examples of large eruptions include the Plinian deposits of 122 BC eruption of Etna, Italy (Coltelli et al. 1998; Houghton et al. 2004; Sable et al. 2006), ~60 ka Fontana Lapilli and ~2-ka Masaya Triple Layer in Nicaragua (Pérez and Freundt 2006; Wehrmann et al. 2006; Costantini et al. 2009, 2010) and the 1886 Tarawera eruption, New Zealand (Walker et al. 1984; Houghton et al. 2004; Sable et al. 2009).

In this study, we investigated the Plinian event associated with the 122 BC eruption of Etna. For this eruption, maximum column height of 24–26 km and average mass eruption rate of $5.0–8.5 \times 10^7$ kg/s have been estimated (Carey and Sparks 1986; Coltelli et al. 1998). Coltelli et al. (1998) divided the 122 BC deposit into seven units,

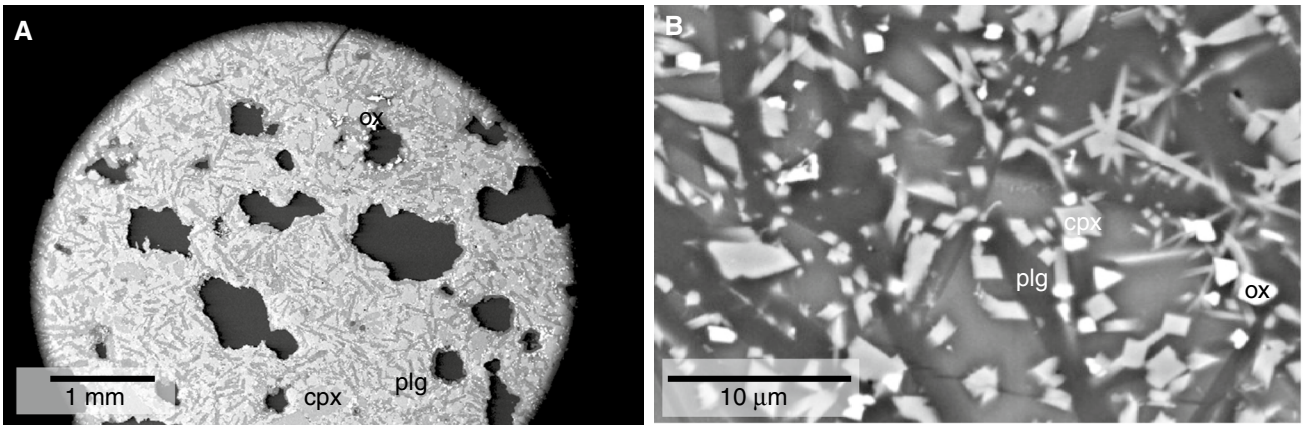

Fig. 5 Representative SEM BSE images for Etna 122 BC eruption at 20 and ×700 magnifications. Plagioclase (*dark gray*) and clinopyroxene (*light gray*) phases are indicated

A–G, with a total volume of 0.285 km^3. Unit A is a Strombolian fallout overlain by a yellowish fine ash tuff of unit B interpreted as a phreatomagmatic deposit. The Plinian phase immediately follows associated with scoriaceous and lithic lapilli deposits forming units C and E, separated by a phreatomagmatic episode (unit D). The final episodes are characterized by phreatomagmatic activity with surge component (unit F) and a late-stage phreatic activity (unit G). Here we focus on the Plinian Member C, a well-sorted scoria preceded and followed by periods of weaker phreatomagmatic activity, which represent the more explosive and thick event of the entire eruption.

Textural characterization and decompression rates

Clasts from the unit C of the eruption of the size range chosen (−2/−3 ϕ) were used for density measurements, performed by a combination of He pycnometer and hydrostatic balance (see detail in Supplementary material). Microphotographs of representative samples are reported in Fig. 5. We calculated total VNDs ranging from 6.8×10^6 cm^{-3} to 2.3×10^7 cm^{-3}, and we compared them with the literature data from Sable et al. (2006). The authors report quantitative studies of textural diversity in the pyroclasts from multiple stratigraphic levels in the Etna 122 BC Plinian units of the deposit. Their total VNDs range from 3×10^6 cm^{-3} to 9×10^7 cm^{-3}, in perfect agreement with our results. We thus recalculated VNDs in the 0.001–0.010 mm diameter to capture the decompression rates during the final stages of ascent, and we obtained values ranging from 9.3×10^6 cm^{-3} to 4.8×10^7 cm^{-3}. In the Toramaru (1995, 2006) equations, used to determine decompression rates, we adopted a surface tension value equal to 0.035 N/m, in agreement with values for dacites of Mourtada Bonnefoi and Laporte (2004) (for similar water and alkali content). This leads to a possible overestimation of the real surface tension which, for the Etna case, ranges between 0.01 ($dP/dt = 1.4$ MPa/s) and 0.035 N/m ($dP/dt = 2.2$ MPa/s). The effect of the variation in surface tension values in the calculated dP/dt and in the eruption dynamics is discussed in the results section. Resulting maximum decompression rates dP/dt for the Etna 122 BC eruption range from 1.68 to 2.72 MPa/s. The mineralogical assemblage is constituted by plagioclase, clinopyroxene and minor olivine. The overall crystal content is an average of $\phi = 0.43$ ($\phi = 0.28$ phenocrysts and $\phi = 0.15$ microlites) with a mean aspect ratio $\bar{R} = 4$ for phenocrysts and microlites, in agreement with previous estimates (Sable et al. 2006).

Model input and output data analysis

In all simulations (Figs. 6, 7), we considered an initial temperature $T = 1100$ °C (Goepfert and Gardner 2010), initial $H_2O = 1.85$ wt% (Del Carlo and Pompilio 2004), 20-m-diameter and 6-km-deep conduit (Patanè et al. 2013) and the initial pressure as lithostatic at 150 MPa. Input parameters, together with the anhydrous chemical composition of the hawaiitic liquid, are presented in Table 3. In all simulations, unless otherwise specified, the strain rate fragmentation (Papale 1999) and the equilibrium degassing mode are adopted. Decompression rate simulations are performed adopting a mean value of dP/dt of 2.2 MPa/s. We run two sets of simulations, with or without the contribution of the microlites.

The following subsections highlight the effects of our software improvements, each one presenting a different comparison of models run with a single change in input parameter (Table 4):

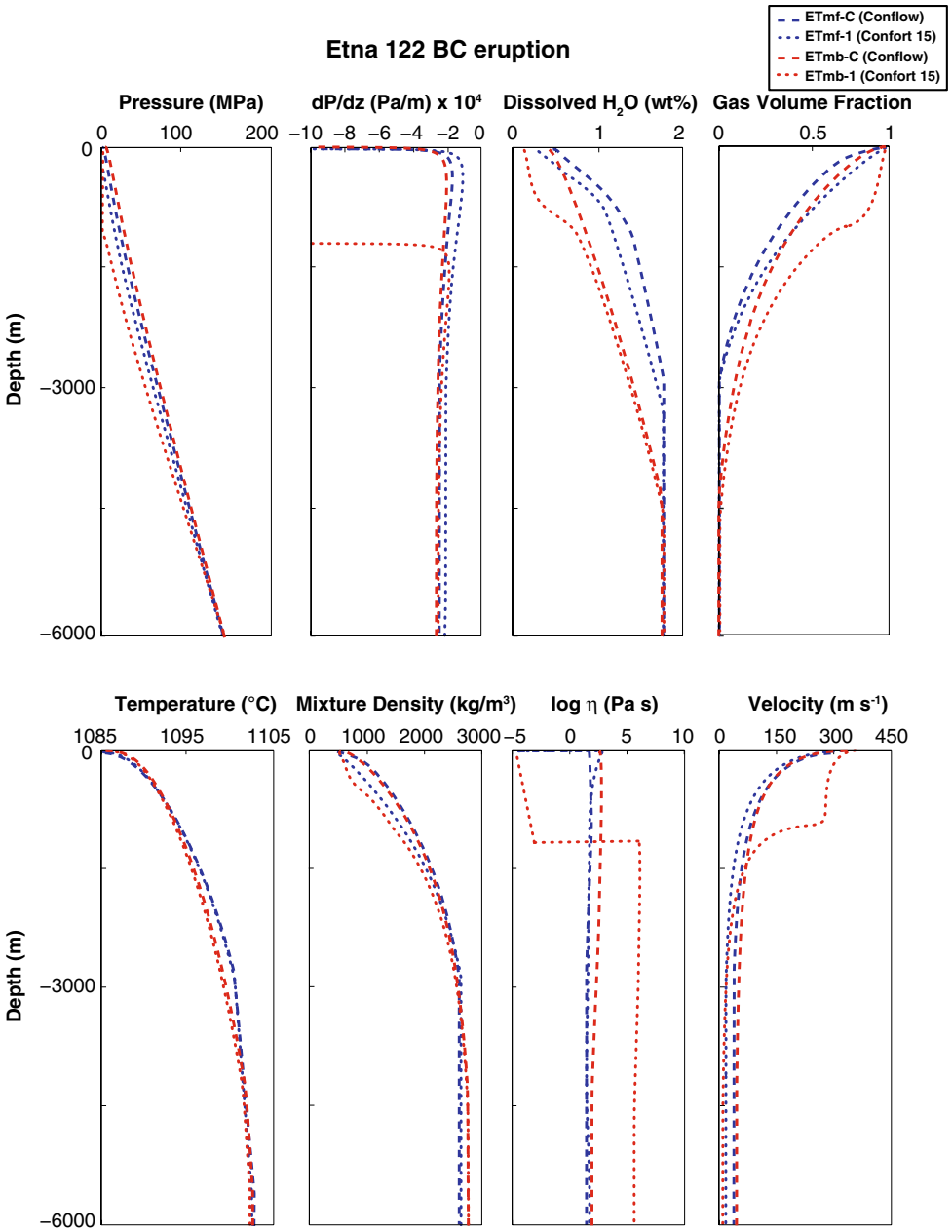

Fig. 6 Plot results for the simulations of both Etna 122 BC "microlite-free" (*blue lines*) and "microlite-bearing" (*red lines*) using the strain rate fragmentation criterion. *Dashed* and *dotted lines* indicate *Conflow* and *Confort 15* models, respectively, without input d*P*/d*t*. Run conditions are: $H_2O_{init} = 1.85$ wt%, $T_{init} = 1100$ °C, $P_{init} = 150$ MPa, conduit diameter = 20 m, conduit length = 6 km. Simulations are labeled according to Table 4

Rheology

(a) Numerical simulations for the "microlite-bearing" system ($\phi = 0.43$) performed applying the *Conflow* and *Confort 15* programs without d*P*/d*t* input (ETmb-C vs. ETmb-1, Fig. 6 dashed and dotted red lines, respectively) show differences in viscosity due the different parameterizations used. In Fig. 8a, liquid viscosity values pertaining to the Etna 122 BC eruption at $T = 1100$ °C are reported as a function of the water content for both Shaw (1972) and Giordano et al. (2008) models (*Conflow* vs. *Confort 15*). The discrepancy between the two parameterizations is highest for anhydrous conditions, with a difference of 0.8 log units Pa s. At the initial water content assumed in the simulations (1.85 wt%), the divergence is about 0.12 log units Pa s (Shaw vs. GRD = 1.72 vs. 1.60 log units Pa s). Older viscosity parameterizations used in the *Conflow* models (Shaw 1972 and ER combination) underestimate not only the magmatic liquid viscosity, but especially and to great extent the crystal-bearing bulk viscosity (Fig. 8b). The ER equation does not consider the strong effect of crystal shape on viscosity, which is especially important for the elongated plagioclases typical of the Etna 122 BC eruption (taken into consideration in *Confort 15* with the Vona et al. 2011 equation).

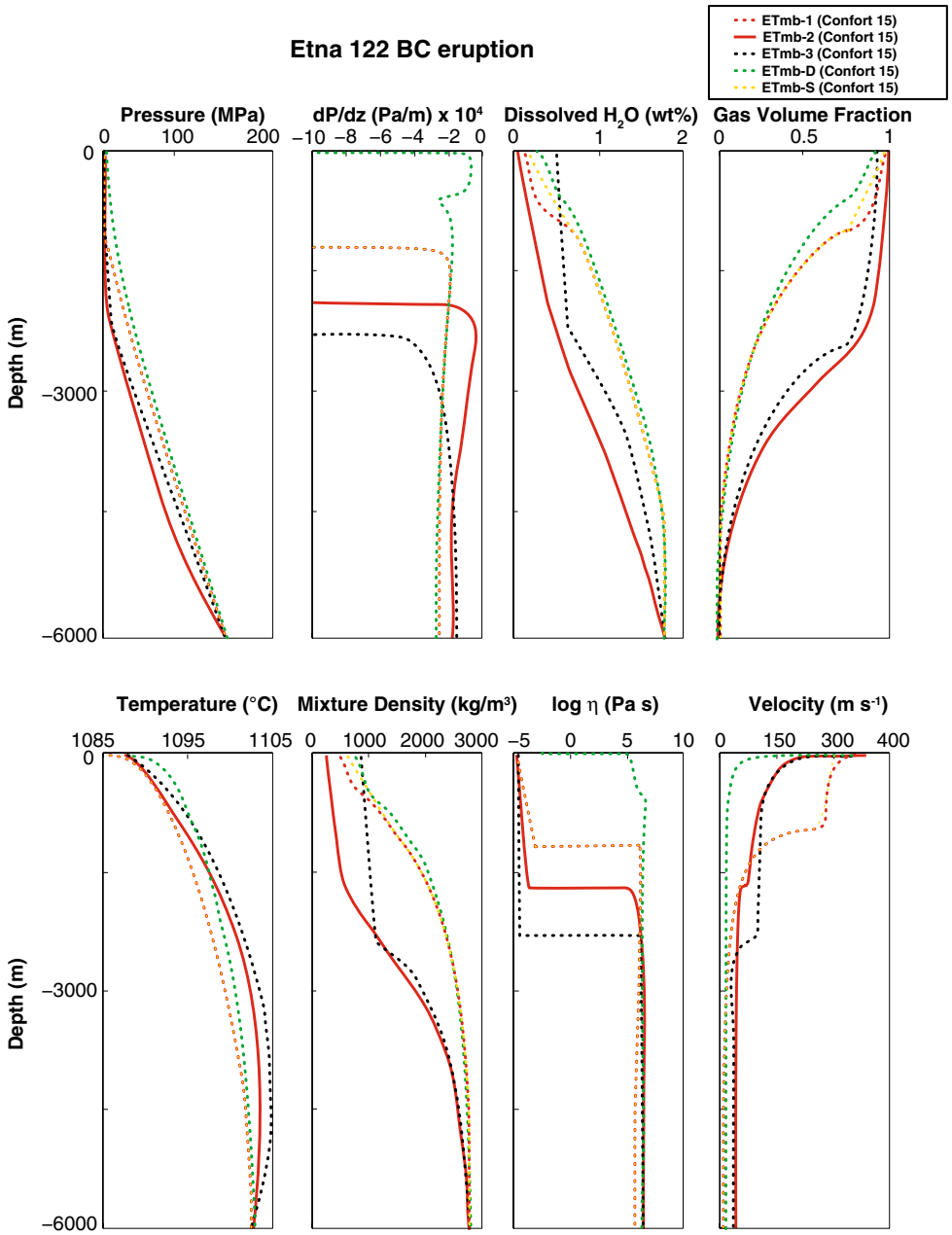

Fig. 7 Plot results for the simulations of Etna 122 BC "microlite-bearing" applying *Confort 15* program. Simulations are: without input d*P*/d*t* (*red dotted*); imposing d*P*/d*t* (*red solid*); porosity criterion (*black*); disequilibrium and overpressure criterion (*green*); stop exsolution after fragmentation (*yellow*). Run conditions are: $H_2O_{init} = 1.85$ wt%, $T_{init} = 1100$ °C, $P_{init} = 150$ MPa, conduit diameter = 20 m, conduit length = 6 km. Simulations are labeled according to Table 4

In this case, the discrepancy between ER (*Conflow*) and Vona et al. (2011) (*Confort 15*) parameterization is dramatic, yielding a difference in resulting relative viscosity of about 3.2 log units (1.3 vs. 4.5 log units Pa s). The *Conflow* rheological model for these conditions is inaccurate (at crystallinity above 30 vol% Newtonian assumption and the Marsh (1981) calibration of the Einstein–Roscoe equation are not valid). We decided to run the simulation in any case, although inaccurate, in order to be able to compare the results with the new *Confort 15* modeling.

The updates unique in *Confort 15* in this case have pivotal implications for eruption dynamic and the achievement of fragmentation conditions, which are not reached in the *Conflow* simulation, despite the higher crystal concentration. This indicates that high crystal content alone is not a sufficient prerequisite to allow for fragmentation to occur. The elongated crystal shape, taken into account in the viscosity parameterization used in *Confort 15*, promotes the dramatic viscosity increase ($10^{6.8}$ vs. $10^{3.1}$ Pa s) leading to explosive fragmentation of the magmatic mixture. In *Confort 15* (ETmb-1), the

Table 3 Input data for the Etna 122 BC performed simulations

Input parameters	Etna 122 BC
Chemical composition (wt%)[a]	
SiO_2	49.32
TiO_2	1.95
Al_2O_3	18.44
Fe_2O_3	7.80
FeO	3.01
MnO	0.18
MgO	2.78
CaO	9.39
Na_2O	4.18
K_2O	1.72
P_2O_5	0.5
Water content (wt%)[b]	1.85
Phenocrysts[c]	
Plagioclase	0.19 (AR = 5)
Clinopyroxene	0.05 (AR = 3)
Olivine	0.04 (AR = 2)
Microlites[c]	
Plagioclase	0.07 (AR = 5)
Clinopyroxene	0.08 (AR = 3)
Temperature (°C)[d]	1100
Initial pressure (MPa)[e]	150
Decompression rate (MPa/s)[f]	2.2
Conduit diameter (m)[g]	20
Conduit length (m)[g]	6000

[a] Melt compositions from Coltelli et al. (1998)

[b] Water content from Del Carlo and Pompilio (2004)

[c] Crystals (phenocrysts plus microlites) calculated in this study. In *Conflow*, phenocrysts and microlites are summed in a single phase and no aspect ratio is assigned

[d] Temperature from Goepfert and Gardner (2010)

[e] Initial pressure assumed as lithostatic (see text for details)

[f] Decompression rates calculated in this study, utilized only in *Confort 15*

[g] Conduit and length diameter from Patanè et al. (2013)

much higher viscosity leads to the achievement of fragmentation (at 980 m), a three-times lower mass fluxes (3.3×10^3 vs. 0.2×10^8 kg/s) and slightly higher exit velocities (332 vs. 320 m/s), the latter due to enhanced exsolution and lower densities at the exit.

(b) In order to understand how much microlite crystallization affects eruption dynamics, we focus on the comparison between two *Confort 15* simulations, specifically the "microlite-bearing" and "microlite-free" runs (ETmb-1 vs. ETmf-1, Fig. 6, dotted red and blue lines). The large microlite crystallization yields an increase in maximum viscosity of about four orders of magnitude ($10^{6.8}$ vs. $10^{2.8}$ Pa s), which leads to brittle fragmentation conditions (at 980 m). In ETmb-1, the increased viscosity is responsible for stronger frictional forces at the conduit walls with a decrease in velocities along the conduit and in the mass flux (3.2×10^3 vs.1×10^5 kg/s). The net effect is a low average pressure within the conduit up to the exit (4.12 vs. 4.72 MPa), higher degree of exsolution, lower residual water (0.31 vs. 0.33 wt%) and lower densities where microlites are present. Porosities at fragmentation agree well with image-derived porosities for ETmb-1 (66 vs. 70 %) allowing us to more confidently apply our results to the interpretation of the natural case. As observed in previous simulations, higher viscosities (ETmb-1) lead to slightly higher exit velocities (332 vs. 318 m/s), due to enhanced exsolution and resulting higher gas volume fraction (99 vs. 98 %) and lower densities at the surface than in microlite-free models. Therefore, we conclude that microlites exert a strong control in increasing viscosity and effectively permitting brittle fragmentation of the magma and explosive eruptions.

Decompression rate

(c) In Fig. 7, in order to evaluate the effect of different decompression rates in the Etna 122 BC magma, we compare models using *Confort 15* program, with input decompression rate ($dP/dt = 2.2$ MPa/s, ETmb-2, solid red line) and without dP/dt input (ETmb-1, dotted red line). In this comparison, maximum viscosities achieved along the conduit are identical ($10^{6.9}$ vs. $10^{6.8}$ Pa s), but the faster input decompression rate (ETmb-2) satisfies the strain rate criterion deeper in the conduit (1200 vs. 980 m). Higher decompression rates correspond to lower pressure distributions along the conduit and enhanced volatile exsolution, higher acceleration and higher initial velocities, as in the case of Pantelleria's Green Tuff magmas. Initial velocities are directly correlated with mass fluxes, which are greater in ETmb-2 by about three orders of magnitude (9.2×10^6 vs. 3.3×10^3 kg/s), with important implications in terms of eruption dynamics and stability of the eruptive column, as observed for Pantelleritic magma. In ETmb-2, the pressure path is offset to lower values throughout the conduit up to the exit (3.4 vs. 4.1 MPa). At identical initial water content, exit velocities are correlated with the density and the gas volume fraction at the conduit exit. For ETmb-2, lower pressure values favor an increase in the rate of volatile exsolution and gas expansion and this is reflected in the lower residual water content (0.21 vs. 0.31 wt%) and lower densities and higher velocities (343 vs. 332 m/s). Because of the uncertainty in the choice of the most appropriate surface tension values in the Toramaru calculations (Fig. S1 of Supplementary material) and in order to evaluate the effect of different surface tensions in the final dP/dt values and in the eruption dynam-

Table 4 Summary of main results for the Etna 122 BC performed simulations (for details see text)

Simulation id	Sample	Program	Temperature (°C)	Fragmentation criterion	Decompression rate (MPa/s)	Mass flux (Kg/s)	Initial velocity (m/s)	Initial density (kg/m^3)	Fragmentation depth (m)	Maximum viscosity (log units Pa s)	Exit velocity (m/s)	Residual water (wt%)	Final pressure (MPa)	Final density (kg/m^3)	Exit gas volume fraction
ETmf-C	Microlite-free	Conflow	1100	Strain rate	–	2.4×10^6	22.93	2500	–	2.2	294	0.49	5.45	638	0.98
ETmf-1	Microlite-free	Confort 15	1100	Strain rate	–	1.0×10^5	12.97	2500	–	2.8	318	0.33	4.72	581	0.98
ETmb-C	microlite-bearing	Conflow	1100	Strain rate	–	0.2×10^8	26.17	2650	–	3.1	320	0.48	6.26	538	0.99
ETmb-1	Microlite-bearing	Confort 15	1100	Strain rate	–	3.2×10^3	11.24	2650	980	6.8	332	0.31	4.12	501	0.99
ETmb-2	Microlite-bearing	Confort 15	1100	Strain rate	2.2	9.2×10^6	28.01	2650	1200	6.9	343	0.21	3.42	432	0.99
ETmb-3	Microlite-bearing	Confort 15	1100	0.75 porosity	–	6.4×10^5	15.77	2650	2300	6.8	320	0.53	8.23	920	0.97
ETmb-D	microlite-bearing	Confort 15	1100	Overpressure	–	6.4×10^3	29.12	2650	20	6.9	335	0.42	5.15	542	0.98
ETmb-S (se[a])	Microlite-bearing	Confort 15	1100	Strain rate	–	3.0×10^3	10.92	2650	970	6.8	312	0.38	4.10	523	0.98
ETmb-st[b]	Microlite-bearing	Confort 15	1100	Strain rate	1.4	6.1×10^6	25.11	2650	1080	6.8	339	0.27	3.78	484	0.99

[a] se = stop exsolution at/after fragmentation

[b] Simulation considering a surface tension = 0.01 N/m and a corresponding $dP/dt = 1.4$ MPa/s

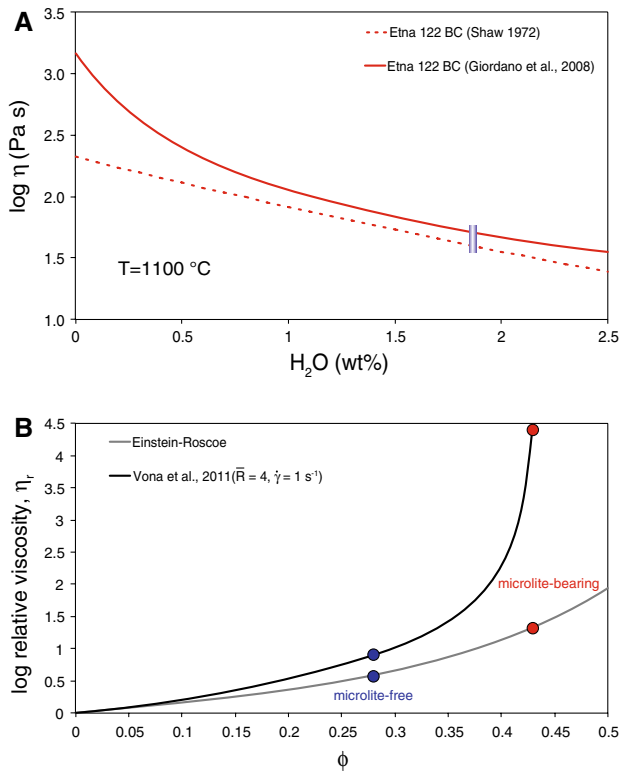

Fig. 8 Crystal-free and crystal-bearing rheology of the Etna 122 BC eruption. **a** Calculated liquid viscosity as a function of the water content for all used viscosity parameterizations (Shaw 1972; Giordano et al. 2008). Blue area indicates initial H_2O content assumed in the simulations (1.85 wt%). **b** Relative viscosity of the multiphase magma as a function of crystal fraction (ϕ). *Gray line* describes the Einstein–Roscoe equation (ER), *black line* the model by Vona et al. (2011). *Circles* represent viscosity estimations based on measured crystallinity for the microlite-free (*blue*) and microlite-bearing (*red*) case

ics, we performed the additional simulation ETmb-st identical to the Etna case ETmb-2, but considering dP/dt = 1.4 MPa/s (the minimum decompression rate). In this case, the fragmentation level raises from 1200 to 1080 m, corresponding to higher pressure distributions (3.42 vs. 3.78 MPa) and lower final velocities (343 vs. 339 m). Data are reported in Table 4.

Fragmentation criteria

(d) Simulations adopting different fragmentation criteria are also presented in Fig. 7. Run ETmb-3 (dotted black line) adopting porosity threshold is compared to ETmb-1 (strain rate fragmentation criterion, dotted red line). Both runs do not constrain ascent rate (no dP/dt input). As in the case of the Green Tuff magmas, fragmentation considering the porosity criterion (ETmb-3, black line) occurs more than twice as deep in the conduit with respect to simulations relative to the case of strain rate fragmentation (2300 vs. 980 m). Porosity and strain rate criteria reach identical maximum viscosity ($10^{6.8}$ Pa s), as the initial path of degassing up to fragmentation condition is almost identical. Mass fluxes are two orders higher in ETmb-3 (6.4×10^5 vs. 3.2×10^3 kg/s). Final pressure and residual water content are also higher, and resulting exit velocities are slightly lower (320 vs. 332 m/s). As in the case of Pantelleritic magmas, the higher mass flux in the 0.75 porosity case is correlated with the higher fragmentation depth achieved applying the porosity fragmentation criterion. At higher depth, mixture viscosity is much lower and this leads to higher pressure at the exit, higher exit densities (and higher residual water content) and hence higher mass eruption rate.

Disequilibrium bubble growth

(e) A set of simulations applying the disequilibrium mode are performed (ETmb-D, Fig. 7 dotted green line) and compared to the relative equilibrium run (ETmb-1, dotted red line) for microlite-bearing melts. In the disequilibrium mode, once the viscous limit is reached, testified by a very large Peclet number, *Confort 15* calculates the disequilibrium average bubble radius (Eqs. 2, 3). As the bubble growth is delayed, due to the viscous forces, overpressure in bubbles with respect to the surrounding liquid is developed. In ETmb-D, growing bubbles start to build up overpressure during ascent at about 7 MPa corresponding to about 600 m depth. The overpressure leads to fragmentation at very shallow conditions (~20 m depth). To achieve choked flow at the vent, initial velocities are strongly increased (29 vs. 11 m/s) reflecting higher mass fluxes (6.4×10^3 vs. 3.2×10^3 kg/s). Moreover, the bubble growth delay leads to a higher pressure path up to the exit (5.15 vs. 4.12 MPa), lower final gas volume fraction and higher residual water content. In general, however, as for the Pantelleria case, disequilibrium bubble growth initiates at very shallow conditions near the surface, at porosities on the order of 96 %. Fragmentation conditions are reached at even shallower depth in the conduit, at porosity of about 97 %. Fragmentation according to porosity and strain rate criteria both occurs before the onset of disequilibrium conditions, for porosities more comparable to values reported in textural studies (75–90 %). For this reason, we suggest that, at least for the eruptions analyzed in this study, the assumption of equilibrium degassing is reasonable and can be adopted for the modeling of the eruption dynamics.

Gas exsolution at/after fragmentation

(f) *Confort 15* allows the option of calculating continued exsolution above the fragmentation depth or terminating it at fragmentation level. In Fig. 7, ETmb-S (i.e., exsolution stopped at fragmentation, dotted yellow line) is compared to ETmb-1 (exsolution continuing up to the

vent, dotted red line). As in the case of the Green Tuff magmas, interrupting the exsolution at fragmentation leads to slightly lower initial and final velocities (10.92 vs. 11.24 m/s and 312 vs. 332 m/s), slightly lower mass fluxes (3.0×10^3 vs. 3.2×10^3 kg/s) and slightly higher residual water content at the exit (0.38 vs. 0.31 wt%). As for the case of Green Tuff *Member A*, allowing exsolution to proceed after fragmentation or to terminate at fragmentation level does not produce any remarkable difference in eruptive dynamics.

Discussion

In agreement with *Conflow* model results, *Confort 15* models show that temperature, composition and volatile content exert primary controls on the depth of fragmentation, flow velocity, pressure within the conduit and exsolution level. In addition, we have shown here that updates unique to *Confort 15* are able to quantify the strong effect of bulk viscosity (liquid and crystals) on flow parameters. We have also demonstrated that decompression rate values based on textural information can constrain fragmentation depth and mass flux.

Some important considerations inferred from our simulations under equilibrium degassing conditions are here summarized:

(a) an increase in magma viscosity due to melt composition/crystallinity (crystal content and crystal shape) at constant initial water content causes a decrease in the pressure along the conduit, thereby enhancing water exsolution and degassing, leading to a deepening of the fragmentation level (consistent with the results of Papale et al. 1998);
(b) an increase in viscosity due to melt composition/crystallinity (crystal content and crystal shape) corresponds to a decrease in mass flux, consistent with basic fluid mechanics principles and with inferred eruptive changes in cases where magma composition varies over a small timescale (Neri et al. 1998);
(c) VND-based decompression rates are consistently higher than those calculated from models and in good agreement with the literature values (up to 4.9 MPa/s for the Izu-Oshima, Toramaru 2006; between 6.3 and 91 MPa/s for Towada, Toramaru 2006; up to 12.75 MPa/s for the Vesuvius 79 AD, Shea et al. 2010b; up to 12.1 for the Chaitén 2008, Alfano et al. 2012; up to 35 MPa/s for the Macauley Volcano, Shea et al. 2013). Adjusting models to agree with these rates causes a deepening of fragmentation depth accompanied by an increase in velocity and in the mass flux of the mixture, enhanced exsolution and a decrease in the density of the magmatic mixture at the exit;
(d) the use of a 0.75 porosity fragmentation threshold results consistently in deeper fragmentation depths than those obtained using a strain rate-dependent fragmentation criterion and higher mass eruption rate;
(e) in all simulations, porosities at fragmentation compare well with porosity derived from image analysis, with an estimated error of ± 10 %.

In general, the good agreement between the porosities calculated and derived from image analyses underscores the importance to constrain numerical simulation with input data derived from field observations and textural analyses of juvenile samples especially whenever numerical simulation results are to be directly used to interpret natural cases.

The good correlation found in this study gives us more strength and confidence to draw some considerations for the dynamic of Pantelleria and Etna eruptions.

In all Pantelleria simulations, exit velocities are mostly governed by the exsolution path, and for identical water content, exit velocity variation is limited. Simulation results indicate that the tendency of pantelleritic magmas (*Member A*) to brittly fragment or to effusively flow is a function of the initial temperature, coupled with the crystal content of the melt. In fact, at high temperature (950 °C) and low crystal content ($\phi = 0.08$), the magma does not reach fragmentation conditions and the simulation suggests effusive flow of magma.

Although lack of fragmentation below the Earth's surface does not necessarily indicate a transition from explosive to effusive behavior (e.g., Legros and Kelfoun 2000), such a transition is likely in most cases. The ability of peralkaline magmas to shift between explosive and effusive eruptions seems therefore to be mainly related to temperature variations. This characteristic is unique among silicic magmas and differs from normal behavior of peraluminous or metaluminous silicic magmas such as trachyte or rhyolites. This behavior derives from the peculiar viscosity versus temperature curve of peralkaline magmas. Previous studies (Di Genova et al. 2013) have demonstrated that peralkaline rhyolites have low fragility and present a very high viscosity at high temperatures, comparable with their metaluminous counterparts and in agreement with their low NBO/T. However, at low temperatures, their viscosity is lower than metaluminous rhyolites and trachytes and lower than most natural melts, and this has been attributed to the effect of alkalis in increasing the number of configurational states of the liquid and therefore decreasing configurational entropy and viscosity (Di Genova et al. 2013). As a consequence of this, in the range of magmatic temperatures, the viscosities of the liquids vary from very low (950 °C, $\eta = 10^4$ Pa s, lower than the metaluminous magmas) to moderately high values (750 °C, $\eta = 10^6$ Pa s), allowing

for the observed shift between explosive ad effusive eruptions, as evidenced by the wide spectrum of eruptive styles and intensities which can be typically found at Pantelleria Island. Moreover, the relatively high eruptive temperatures (750 °C), moderate viscosities at fragmentation observed in this study (on the order of 10^6 Pa s) and low glass transition temperatures (418–552 °C, Di Genova et al. 2013) of these chemically peculiar magmas may be held responsible for the extended welding and large-scale rheomorphic structures commonly associated with pantelleritic deposits (e.g., Wolff and Wright 1981; Mahood 1984; Stevenson and Wilson 1997).

Also in the case of Etna 122 BC Plinian eruption, the viscosity seems to be a first-order parameter in controlling the magma ascent dynamics along the conduit. Although the high explosivity of low-viscosity mafic magmas may seem counterintuitive, there are several explanations for this peculiar behavior. Triggering mechanisms hypothesized for highly explosive mafic eruptions commonly include a general increase in crystallinity with a subsequent change in bulk viscosity (e.g., Lejeune and Richet 1995; Papale 1999; Sable et al. 2006), water–magma interaction (e.g., Dellino et al. 2004; Houghton et al. 2004; D'Oriano et al. 2005), flushing of CO_2 (e.g., Iacono Marziano et al. 2007; Freda et al. 2010; Iacovino et al. 2013) and high rates of syn-eruption decompression (e.g., Klug et al. 2002; Pardo et al. 2009). For the case analyzed in this study, Etna 122 BC, instantaneous decompression accompanying unloading due to caldera collapse or flank instability (Coltelli et al. 1998) was hypothesized, although other authors did not find conclusive evidence of contemporaneous slope failure (Houghton et al. 2004). Sable et al. (2009) suggested that the high microlite content in the magmatic mixture may have played a fundamental role in driving the Plinian Etna 122 BC eruption. Our study can help shed some light on the interpretation of this highly energetic basaltic eruption. The results presented clearly indicate that microlite-free simulations do not reach brittle failure and therefore explosive behavior. Increasing the overall crystal content, considering the microlite contribution and taking into account the elongated shapes of crystals by using Vona et al. (2011) parameterization, leads to a strong increase in viscosity. This allows the magma to erupt explosively, reaching the brittle fragmentation conditions at viscosities of $10^{6.8}$ Pa s. Decompression rates calculated on the basis of the textural analysis and the Toramaru decompression rate meter suggest that this magma was subjected to rapid decompression associated with rapid ascent which further promoted explosive fragmentation and Plinian activity with calculated mass fluxes in accordance with this highly energetic eruption (10^6 kg/s). Our results quantitatively demonstrate, for the first time, as suggested by Houghton et al. (2004), Sable et al. (2006) and Moitra et al. (2013), that microlite crystallization can increase the magma's effective viscosity and allow Plinian activity even in the case of commonly effusive basaltic magmas.

Considering disequilibrium bubble growth, at pressure up to 10 MPa for GT and 7 MPa for ET, bubble growth becomes viscously limited, as a consequence of H_2O exsolution and increasing viscosity. Consequently magma pressure decreases more rapidly than gas pressure inside the bubbles, leading to a pressure build-up inside the vesicles. The bubble overpressure reaches the fragmentation threshold pressure (i.e., according to the overpressure fragmentation criterion; Spieler et al. 2004) for both eruptions, in the shallowest part of the conduit (up to the last 20 m) at a ΔP of about 1 MPa. Due to the very superficial depths of fragmentation, in order to achieve choked flow conditions, initial velocities and mass fluxes increase by a factor of 2–2.5, in agreement with Mangan et al. (2004).

In general, disequilibrium degassing, for the compositions analyzed in this study, initiates at very shallow conditions near the surface and porosities over 90 %. Fragmentations according to porosity and strain rate criteria both occur before the onset of disequilibrium conditions, for porosities more comparable to values reported in textural studies. For this reason, we suggest that, at least for the eruptions analyzed and the viscosity range investigated in this study, the assumption of equilibrium degassing is reasonable and can be preferred over the disequilibrium bubble growth.

General classification schemes define different eruptive styles mostly based on magma silica content (SiO_2), assuming that low silica content magmas are more prone to produce less explosive (effusive) eruptions and, on the opposite, silica-rich melts generally erupt more explosively for a combination of viscosity and volatile content variations. In this study, we chose two compositional end-members (basalts vs. peralkaline rhyolite) and demonstrated that viscosity variations play a more subtle role in determining eruptive behavior, yielding volcanoes to experience atypical eruptions. Considering all distinct peculiarities of analyzed magmas, effective viscosity of peralkaline rhyolite may be lower than basalts leading to possible effusive behavior, welding and rheomorphism processes. On the other hand, highly crystalline mafic magmas can develop very high viscosities generating highly explosive Plinian activity, mimicking their more acidic counterparts.

Conclusions

In this study, we present *Confort 15,* an updated version of the *Conflow* (Mastin and Ghiorso 2000) open-source

numerical model for flow of magma and gas in eruptive conduits during steady-state pyroclastic eruptions. A new calculation of decompression rate using vesicle number densities (VNDs) obtained from textural analyses and Toramaru (1995, 2006) equations is introduced. Rheological parameters are also updated, inserting the most recent constitutive equations (Giordano et al. 2008; Costa et al. 2009; Vona et al. 2011; Di Genova et al. 2013) concerning both the liquid and crystal-bearing rheology.

Our improvements allow users to derive more correct viscosity values for metaluminous and peraluminous liquids, to extend the new model to peralkaline liquids and to crystal-bearing magmas expanding the range of applicability to crystal fractions excluded in *Conflow* (>30 vol%). Improved rheological equations take into consideration not only the crystal content, but also the crystal shape and the strain rate in the evaluation of the viscosity of the magmatic mixture. This aspect plays a primary role in influencing the conduit dynamics, promoting the viscosity increase and strongly affecting the fragmentation occurrence and the related flow properties. Application of textural-derived VNDs, different fragmentation criteria and disequilibrium degassing simulations also results in more plausible prediction of flow scenarios.

In order to appreciate the potential of the new program and to evaluate viscosity variations and how much they affect the eruptive dynamic along the conduit, both *Conflow* and *Confort 15* versions were applied to two natural cases: the Green Tuff eruption, Pantelleria (the opening peralkaline and the trachytic ending phases), and the Plinian Etna 122 BC eruption.

Decompression rates, magma rheology and fragmentation are controlling inputs to all models of magmatic flow and are therefore crucial to our understanding of the magmatic processes and to our ability to predict volcanic hazards.

All aspects considered in the modeling of the eruptive scenario align to make a great step forward in the modeling capabilities of the program and to strongly improve the predictive power of the code. The *Confort 15* presented program is written in Fortran 90 and can be compiled on any platform that has such a compiler. The source code to this model and its manual are posted on https://vhub.org/resources/3743.

Acknowledgments We thank Heather Wright for her careful and thorough review which greatly helped improving the manuscript. We are grateful to Atsushi Toramaru and Thomas Shea for the assistance with decompression rate calculations. We like to thank Marco Viccaro for providing some Pantelleria samples. We thank Chiara Montagna and an anonymous reviewer for supporting comments on an earlier version of this manuscript. Thomas Giachetti and an anonymous reviewer are also acknowledged for their constructive and careful reviews.

References

Alfano F, Bonadonna C, Gurioli L (2012) Insights into eruption dynamics from textural analysis: the case of the May, 2008, Chaitén eruption. Bull Volcanol 74:2095–2108. doi:10.1007/s00445-012-0648-3

Alidibirov MA (1994) A model for viscous magma fragmentation during volcanic blasts. Bull Volcanol 56:459–465. doi:10.1007/BF00302827

Bagdassarov NS, Dingwell DB (1992) A rheological investigation of vesicular rhyolite. J Volcanol Geotherm Res 50:307–322

Bagdassarov NS, Dingwell DB (1993) Deformation of foamed rhyolites under internal and external stresses: an experimental investigation. Bull Volcanol 55:147–154

Bagdassarov NS, Dorfman A, Dingwell DB (2000) Effect of alkalis, phosphorus, and water on the surface tension of haplogranite melt. Am Mineral 85:33–40

Bottinga Y, Weill D (1970) Densities of liquid silicate systems calculated from partial molar volumes of oxide components. Am J Sci 269:169–182

Bursik MI, Woods AW (1996) The dynamics and thermodynamics of large ash flows. Bull Volcanol 58:175–193. doi:10.1007/s004450050134

Carey S, Sparks RSJ (1986) Quantitative models of the fallout and dispersal of tephra from volcanic eruption columns. Bull Volcanol 48:109–125

Caricchi L, Giordano D, Burlini L, Ulmer P, Romano C (2008) Rheological properties of magma from the 1538 eruption of Monte Nuovo (Phlegrean Fields, Italy): an experimental study. Chem Geol 256:158–171. doi:10.1016/j.chemgeo.2008.06.035

Catalano S, Tortorici L, Viccaro M (2014) Regional tectonic control on large size explosive eruptions: Insights into the Green Tuff ignimbrite unit of Pantelleria. J Geodyn 73:23–33. doi:10.1016/j.jog.2013.10.008

Civetta L, D'Antonio M, Orsi G, Tilton GR (1998) The geochemistry of volcanic rocks from Pantelleria Island, sicily channel: petrogenesis and characteristics of the mantle source region. J Petrol 39:1453–1491. doi:10.1093/petroj/39.8.1453

Civile D, Lodolo E, Tortorici L, Lanzafame G, Brancolini G (2008) Relationships between magmatism and tectonics in a continental rift: The Pantelleria Island region (Sicily Channel, Italy). Mar Geol 251:32–46. doi:10.1016/j.margeo.2008.01.009

Cluzel N, Laporte D, Provost A, Kannewischer I (2008) Kinetics of heterogeneous bubble nucleation in rhyolitic melts: implications for the number density of bubbles in volcanic conduits and for pumice textures. Contrib Mineral Petrol 156:745–763

Coltelli M, Del Carlo P, Vezzoli L (1998) Discovery of a Plinian basaltic eruption of Roman age at Etna volcano, Italy. Geology 26:1095–1098

Cordonnier B, Hess KU, Lavallée Y, Dingwell DB (2009) Rheological properties of dome lavas: Case study of Unzen volcano. Earth Planet Sci Lett 279:263–272. doi:10.1016/j.epsl.2009.01.014

Costa A, Melnik O, Vedeneeva E (2007) Thermal effects during magma ascent in conduits. J Geophys Res 112:1–16. doi:10.1029/2007jb004985

Costa A, Caricchi L, Bagdassarov NS (2009) A model for the rheology of particle-bearing suspensions and partially molten rocks. Geochem Geophys Geosyst 10:1–13. doi:10.1029/2008gc002138

Costantini L, Bonadonna C, Houghton BF, Wehrmann H (2009) New physical characterization of the Fontana Lapilli basaltic Plinian eruption, Nicaragua. Bull Volcanol 71:337–355. doi:10.1007/S00445-008-0227-9

Costantini L, Houghton BF, Bonadonna C (2010) Constraints on eruption dynamics of basaltic explosive activity derived from

chemical and microtextural study: The example of the Fontana Lapilli Plinian eruption, Nicaragua. J Volcanol Geotherm Res 189:207–224. doi:10.1016/j.jvolgeores.2009.11.008

D'Oriano C, Poggianti E, Bertagnini A, Cioni R, Landi P, Polacci M, Rosi M (2005) Changes in eruptive style during the A.D. 1538 Monte Nuovo eruption (Phlegrean Fields, Italy): the role of syn-eruptive crystallization. Bull Volcanol 67:601–621. doi:10.1007/s00445-004-0397-z

de' Michieli Vitturi M, Clarke AB, Neri A, Voight B (2010) Transient effects of magma ascent dynamics along a geometrically variable dome-feeding conduit. Earth Planet Sci Lett 295:541–553. doi:10.1016/j.epsl.2010.04.029

Del Carlo P, Pompilio M (2004) The relationship between volatile content and the eruptive style of basaltic magma: the Etna case. Ann Geophys 47:1–10

Dellino P, Isaia R, La Volpe L, Orsi G (2004) Interaction between particles transported by fallout and surge in the deposits of the Agnano-Monte Spina eruption (Campi Flegrei, Southern Italy). J Volcanol Geotherm Res 133:193–210. doi:10.1016/S0377-0273(03)00398-6

Dellino P, Dioguardi F, Zimanowski B, Büttner R, Mele D, La Volpe L, Sulpizio R, Doronzo DM, Sonder I, Bonasia R, Calvari S, Marotta E (2010) Conduit flow experiments help constraining the regime of explosive eruptions. J Geophys Res 115:1–17. doi :10.1029/2009JB006781

Di Carlo I, Rotolo SG, Scaillet B, Buccheri V, Pichavant M (2010) Phase equilibrium constraints on pre-eruptive conditions of recent felsic explosive volcanism at Pantelleria Island, Italy. J Petrol 51:2245–2276. doi:10.1093/petrology/egq055

Di Genova D, Romano C, Hess KU, Vona A, Poe BT, Giordano D, Dingwell DB, Behrens H (2013) The rheology of peralkaline rhyolites from Pantelleria Island. J Volcanol Geotherm Res 249:201–216. doi:10.1016/j.jvolgeores.2012.10.017

Dingwell DB, Webb S (1989) Structural relaxation in silicate melts and non-Newtonian melt rheology in geologic processes. Phys Chem Miner. doi:10.1007/BF00197020

Dingwell DB, Romano C, Hess KU (1996) The effect of water on the viscosity of a haplogranitic melt under P-T-X conditions relevant to silicic volcanism. Contrib Mineral Petrol 124:19–28. doi:10.1007/s004100050170

Dioguardi F, Dellino P, de Lorenzo S (2013) Integration of large-scale experiments and numerical simulations for the calibration of friction laws in volcanic conduit flows. J Volcanol Geotherm Res 250:75–90. doi:10.1016/j.jvolgeores.2012.09.011

Dobran F (1992) Nonequilibrium flow in volcanic conduits and application to the eruptions of Mt. St. Helens on May 18, 1980, and Vesuvius in AD 79. J Volcanol Geotherm Res 49:285–311. doi:10.1016/0377-0273(92)90019-A

Freda C, Gaeta M, Giaccio B, Marra F, Palladino D, Scarlato P, Sottili G (2010) CO_2-driven large mafic explosive eruptions: the Pozzolane Rosse case study from the Colli Albani Volcanic District (Italy). Bull Volcanol 73:241–256. doi:10.1007/s00445-010-0406-3

Gardner JE, Ketcham RA (2011) Bubble nucleation in rhyolite and dacite melts: temperature dependence of surface tension. Contrib Mineral Petrol 162:929–943. doi:10.1007/s00410-011-0632-5

Gardner JE, Thomas R, Jaupart C, Tait S (1996) Fragmentation of magma during Plinian volcanic eruptions. Bull Volcanol 58:144–162

Ghiorso MS, Sack RO (1995) Chemical mass transfer in magmatic processes IV. A revised and internally consistent thermodynamic model for the interpolation and extrapolation of liquid-solid equilibria in magmatic systems at elevated temperatures and pressures. Contrib Mineral Petrol 119:197–212. doi:10.1007/BF00307281

Giordano D, Russell JK, Dingwell DB (2008) Viscosity of magmatic liquids: a model. Earth Planet Sci Lett 271:123–134. doi:10.1016/j.epsl.2008.03.038

Goepfert K, Gardner JE (2010) Influence of pre-eruptive storage conditions and volatile contents on explosive Plinian style eruptions of basic magma. Bull Volcanol 72:511–521. doi:10.1007/s00445-010-0343-1

Gonnermann HM, Manga M (2007) The Fluid Mechanics Inside a Volcano. Annu Rev Fluid Mech 39:321–356. doi:10.1146/annurev.fluid.39.050905.110207

Gonnermann HM, Manga M (2012) Dynamics of magma ascent in the volcanic conduit. In: Fagents SA, Gregg TKP, Lopes RMC (eds) Modeling volcanic processes, the physics and mathematics of volcanism. Cambridge University Press, pp 55–84

Haar L, Gallagher J, Kell G (1984) NBS/NRC steam tables: thermodynamic and transport properties and computer programs for vapor and liquid states of water in SI units. Hemispheres Publishing, Washington

Hess KU, Dingwell DB (1996) Viscosities of hydrous leucogranitic melts: a non-Arrhenian model. Am Mineral 81:1297–1300

Houghton BF, Wilson L (1989) A vesicularity index for pyroclastics deposits. Bull Volcanol 51:451–462

Houghton BF, Wilson CJN, Del Carlo P, Coltelli M, Sable JE, Carey RJ (2004) The influence of conduit processes on changes in style of basaltic Plinian eruptions: Tarawera 1886 and Etna 122 BC. J Volcanol Geotherm Res 137:1–14. doi:10.1016/j.jvolgeores.2004.05.009

Hurwitz S, Navon O (1994) Bubble nucleation in rhyolitic melts: experiments at high pressure, temperature, and water content. Earth Planet Sci Lett 122:267–280. doi:10.1016/0012-821X(94)90001-9

Iacono Marziano G, Gaillard F, Pichavant M (2007) Limestone assimilation and the origin of CO_2 emissions at the Alban Hills (Central Italy): Constraints from experimental petrology. J Volcanol Geotherm Res 166:91–105. doi:10.1016/j.jvolgeores.2007.07.001

Iacovino K, Moore G, Roggensack K, Oppenheimer C, Kyle P (2013) H_2O–CO_2 solubility in mafic alkaline magma: applications to volatile sources and degassing behavior at Erebus volcano, Antarctica. Contrib Mineral Petrol 166:845–860. doi:10.1007/s00410-013-0877-2

Ishibashi H (2009) Non-Newtonian behavior of plagioclase-bearing basaltic magma: Subliquidus viscosity measurement of the 1707 basalt of Fuji volcano, Japan. J Volcanol Geotherm Res 181:78–88. doi:10.1016/j.jvolgeores.2009.01.004

Ishibashi H, Sato H (2007) Viscosity measurements of subliquidus magmas: Alkali olivine basalt from the Higashi-Matsuura district, Southwest Japan. J Volcanol Geotherm Res 160:223–238. doi:10.1016/j.jvolgeores.2006.10.001

Kawaguchi R, Nishimura T, Sato H (2013) Volcano inflation prior to an eruption: Numerical simulations based on a 1-D magma flow model in an open conduit. Earth Planets Space 65:1477–1489. doi:10.5047/eps.2013.05.005

Klug C, Cashman KV, Bacon CR (2002) Structure and physical characteristics of pumice from the climactic eruption of Mount Mazama (Crater Lake). Or Bull Volcanol 64:486–501. doi:10.1007/s00445-002-0230-5

Lanzo G, Landi P, Rotolo SG (2013) Volatiles in pantellerite magmas: a case study of the Green Tuff Plinian eruption (Island of Pantelleria, Italy). J Volcanol Geotherm Res 262:153–163. doi:10.1016/j.jvolgeores.2013.06.011

Lavallée Y, Hess KU, Cordonnier B, Dingwell DB (2007) Non-Newtonian rheological law for highly crystalline dome lavas. Geology 35:843–846. doi:10.1130/G23594A.1

Legros F, Kelfoun K (2000) Sustained blasts during large volcanic eruptions. Geology 28(10):895–898. doi:10.1130/0091-7613(2000)28<895:sbdlve>2.0.co;2

Lejeune A, Richet P (1995) Rheology of crystal-bearing silicate melts: an experimental study at high viscosities. J Geophys Res 100:4215–4229

Lensky NG, Navon O, Lyakhovsky V (2004) Bubble growth during decompression of magma: experimental and theoretical investigation. J Volcanol Geotherm Res 129:7–22

Lev E, Spiegelman M, Wysocki RJ, Karson JA (2012) Investigating lava fl ow rheology using video analysis and numerical flow models. J Volcanol Geotherm Res 247–248:62–73. doi:10.1016/j.jvolgeores.2012.08.002

Llewellin EW, Manga M (2005) Bubble suspension rheology and implications for conduit flow. J Volcanol Geotherm Res 143:205–217. doi:10.1016/j.jvolgeores.2004.09.018

Mader HM, Llewellin EW, Müller SP (2013) The rheology of two-phase magmas: a review and analysis. J Volcanol Geotherm Res 257:135–158. doi:10.1016/j.jvolgeores.2013.02.014

Mahood GA (1984) Pyroclastic rocks and calderas associated with strongly peralkaline magmatism. J Geophys Res 89:8540. doi:10.1029/JB089iB10p08540

Mangan M, Sisson T (2000) Delayed, disequilibrium degassing in rhyolite magma: decompression experiments and implications for explosive volcanism. Earth Planet Sci Lett 183:441–455

Mangan M, Mastin LG, Sisson T (2004) Gas evolution in eruptive conduits: combining insights from high temperature and pressure decompression experiments with steady-state flow modeling. J Volcanol Geotherm Res 129:23–36. doi:10.1016/s0377-0273(03)00230-0

Marsh BD (1981) On the crystallinity, probability of occurrence, and rheology of lava and magma. Contrib Mineral Petrol 78:85–98

Massol H, Koyaguchi T (2005) The effect of magma flow on nucleation of gas bubbles in a volcanic conduit. J Volcanol Geotherm Res 143:69–88. doi:10.1016/j.jvolgeores.2004.09.011

Massol H, Jaupart C, Pepper DW (2001) Ascent and decompression of viscous vesicular magma in a volcanic conduit. J Geophys Res 106:16223–16240

Mastin LG (1995) A numerical program for steady-state flow of Hawaiian magma-gas mixtures through vertical eruptive conduits. U. S. Geological Survey Open File Report 95-756

Mastin LG (2002) Insights into volcanic conduit flow from an open-source numerical model. Geochem Geophys Geosyst 3:1–18

Mastin LG, Ghiorso M (2000) A numerical program for steady-state flow of magma-gas mixtures through vertical eruptive conduits. U. S. Geological Survey Open File Report 00-209

Maxwell J (1866) On the dynamical theory of gases. J Proc Royal Soc London 15:167–171

Melnik O (2000) Dynamics of two-phase conduit flow of high-viscosity gas-saturated magma: large variations of sustained explosive eruption intensity. Bull Volcanol 62:153–170

Moitra P, Gonnermann HM, Houghton BF, Giachetti T (2013) Relating vesicle shapes in pyroclasts to eruption styles. Bull Volcanol 75:691. doi:10.1007/s00445-013-0691-8

Mourtada-Bonnefoi CC, Laporte D (2004) Kinetics of bubble nucleation in a rhyolitic melt: an experimental study of the effect of ascent rate. Earth Planet Sci Lett 218:521–537

Neave DA, Fabbro G, Herd RA, Petrone CM, Edmonds M (2012) Melting, differentiation and degassing at the Pantelleria volcano, Italy. J Petrol 53:637–663. doi:10.1093/petrology/egr074

Neri A, Papale P, Macedonio G (1998) The role of magma composition and water content in explosive eruptions: 2. Pyroclastic dispersion dynamics. J Volcanol Geotherm Res 87:95–115. doi:10.1016/S0377-0273(98)00102-4

Orsi G, Sheridan MF (1984) The Green Tuff of Pantelleria : rheoignimbrite or rheomorphic fall? Bull Volcanol 47:611–626

Papale P (1999) Strain-induced magma fragmentation in explosive eruptions. Nature 397:425–428

Papale P, Neri A, Macedonio G (1998) The role of magma composition and water content in explosive eruptions 1. Conduit ascent dynamics. J Volcanol Geotherm Res 87:75–93

Patanè D, Aiuppa A, Aloisi M, Behncke B, Cannata A, Coltelli M, Di Grazia G, Gambino S, Gurrieri S, Mattia M, Salerno G (2013) Insights into magma and fluid transfer at Mount Etna by a multiparametric approach: A model of the events leading to the 2011 eruptive cycle. J Geophys Res Solid Earth 118:3519–3539. doi:10.1002/jgrb.50248

Pérez W, Freundt A (2006) The youngest highly explosive basaltic eruptions from Masaya Caldera (Nicaragua): stratigraphy and hazard assessment. Geol Soc Am Spec Pap 412:189–207

Picard D, Arbaret L, Pichavant M, Champallier R, Launeau P (2011) Rheology and microstructure of experimentally deformed plagioclase suspensions. Geology 39:747–750. doi:10.1130/G32217.1

Picard D, Arbaret L, Pichavant M, Champallier R, Launeau P (2013) The rheological transition in plagioclase-bearing magmas. J Geophys Res Solid Earth 118:1363–1377. doi:10.1002/jgrb.50091

Polacci M, Papale P, Del Seppia D, Giordano D, Romano C (2004) Dynamics of magma ascent and fragmentation in trachytic versus rhyolitic eruptions. J Volcanol Geotherm Res 131:93–108. doi:10.1016/S0377-0273(03)00319-6

Pyle DM (1995) Assessment of the minimum volume of tephra fall deposits. J Volcanol Geotherm Res 69:379–382

Sable JE, Houghton BF, Del Carlo P, Coltelli M (2006) Changing conditions of magma ascent and fragmentation during the Etna 122 BC basaltic Plinian eruption: Evidence from clast microtextures. J Volcanol Geotherm Res 158:333–354. doi:10.1016/j.jvolgeores.2006.07.006

Sable JE, Houghton BF, Wilson CJN, Carey RJ (2009) Eruption mechanisms during the climax of the Tarawera 1886 basaltic Plinian eruption inferred from microtextural characteristics of the deposits. Geol Soc Lond Spec Publ IAVCEI 2:129–154

Shaw HR (1972) Viscosities of magmatic silicate liquids: an empirical method of prediction. Am J Sci 272:870–893

Shea T, Houghton BF, Gurioli L, Cashman KV, Hammer JE, Hobden BJ (2010a) Textural studies of vesicles in volcanic rocks: An integrated methodology. J Volcanol Geotherm Res 190:271–289. doi:10.1016/j.jvolgeores.2009.12.003

Shea T, Gurioli L, Larsen JF, Houghton BF, Hammer JE, Cashman KV (2010b) Linking experimental and natural vesicle textures in Vesuvius 79AD white pumice. J Volcanol Geotherm Res 192:69–84. doi:10.1016/j.jvolgeores.2010.02.013

Shea T, Gurioli L, Houghton BF, Cioni R, Cashman KV (2011) Column collapse and generation of pyroclastic density currents during the A.D. 79 eruption of Vesuvius: The role of pyroclast density. Geology 39:695–698. doi:10.1130/G32092.1

Shea T, Hammer JE, First E (2013) Magma balloons or bombs? Nat Geosci 6:802–803. doi:10.1038/NGEO1971

Sparks RSJ (1978) The dynamics of bubble formation and growth in magmas: a review and analysis. J Volcanol Geotherm Res 3:1–37

Sparks RSJ, Wilson L (1982) Explosive volcanic eruptions—V. Observations of plume dynamics during the 1979 Soufrière eruption, St Vincent. Geophys J Int 69:551–570

Speranza F, Di Chiara A, Rotolo SG (2011) Correlation of welded ignimbrites on Pantelleria (Strait of Sicily) using paleomagnetism. Bull Volcanol 74:341–357. doi:10.1007/s00445-011-0521-9

Spieler O, Kennedy B, Kueppers U, Dingwell DB, Scheu B, Taddeucci J (2004) The fragmentation threshold of pyroclastic rocks. Earth Planet Sci Lett 226:139–148. doi:10.1016/j.epsl.2004.07.016

Stevenson RJ, Wilson L (1997) Physical volcanology and eruption dynamics of peralkaline agglutinates from Pantelleria. J Volcanol Geotherm Res 79(1–2):97–122

Toramaru A (1995) Numerical study of nucleation and growth of bubbles in viscous magmas. J Geophys Res 100:1913–1931

Toramaru A (2006) BND (bubble number density) decompression rate meter for explosive volcanic eruptions. J Volcanol Geotherm Res 154:303–316. doi:10.1016/j.jvolgeores.2006.03.027

Valentine G, Wohletz K (1989) Numerical models of Plinian eruption columns and pyroclastic flows. J Geophys Res 94:1867–1887

Vona A, Romano C, Dingwell DB, Giordano D (2011) The rheology of crystal-bearing basaltic magmas from Stromboli and Etna. Geochim Cosmochim Acta 75:3214–3236. doi:10.1016/j.gca.2011.03.031

Vona A, Romano C, Giordano D, Russell JK (2013) The multiphase rheology of magmas from Monte Nuovo (Campi Flegrei, Italy). Chem Geol 346:213–227. doi:10.1016/j.chemgeo.2012.10.005

Walker G, Self S, Wilson L (1984) Tarawera 1886, New Zealand—a basaltic plinian fissure eruption. J Volcanol Geotherm Res 21:61–78

Wehrmann H, Bonadonna C, Freundt A, Houghton BF, Kutterolf S (2006) Fontana Tephra: a basaltic Plinian eruption in Nicaragua. Geol Soc Am Spec Pap 482:209–223

White JC, Parker DF, Ren M (2009) The origin of trachyte and pantellerite from Pantelleria, Italy: insights from major element, trace element, and thermodynamic modelling. J Volcanol Geotherm Res 179:33–55. doi:10.1016/j.jvolgeores.2008.10.007

Williams R (2010) Emplacement of radial pyroclastic density currents over irregular topography : the chemically-zoned, low aspect-ratio Green tuff ignimbite, Pantelleria, Italy. Ph.D. thesis, University of Leicester, pp 232

Williams R, Branney MJ, Barry TL (2013) Temporal and spatial evolution of a waxing then waning catastrophic density current revealed by chemical mapping. Geology 42:107–110. doi:10.1130/G34830.1

Wilson L, Sparks RSJ, Huang TC, Watkins ND (1978) The control of volcanic column heights by eruption energetics and dynamics ash. J Geophys Res 83:1829–1836

Wilson L, Sparks RSJ, Walker D (1980) Explosive volcanic eruptions—IV. The control of magma properties and conduit geometry on eruption behaviour. Geophys J R Astron Soc 63:117–148

Wolff JA, Wright JV (1981) Formation of the Green Tuff, Pantelleria. Bull Volcanol 44:681–690. doi:10.1007/BF02597091

Zhang Y, Behrens H (2000) H_2O diffusion in rhyolitic melts and glasses. Chem Geol 169:243–262. doi:10.1016/S0009-2541(99)00231-4

Zhang Y, Ni H (2010) Diffusion of H, C, and O components in silicate melts. Rev Mineral Geochem 72:171–225. doi:10.2138/rmg.2010.72.5